A typical weather pattern for the ozone pollution events in North China

Cheng Gong[1, 2], Hong Liao[3*]

[1]State Key Laboratory of Atmospheric Boundary Layer Physics and Atmospheric Chemistry (LAPC), Institute of Atmospheric Physics, Chinese Academy of Sciences, Beijing, 100029, China,

[2]University of Chinese Academy of Sciences, Beijing, 100029, China,

[3]Jiangsu Key Laboratory of Atmospheric Environment Monitoring and Pollution Control, Jiangsu Collaborative Innovation Center of Atmospheric Environment and Equipment Technology, School of Environmental Science and Engineering, Nanjing University of Information Science and Technology, Nanjing, 210044, China

Correspondence to: Hong Liao (hongliao@nuist.edu.cn)

Abstract. Ground-level observations, reanalyzed meteorological fields and a 3-D global chemical and transport model (GEOS-Chem) were applied in this study to investigate ozone (O_3) pollution events (OPEs) in North China (36.5°N-40.5°N, 114.5°E-119.5°E) during 2014-2017. Ozone pollution days (OPDs) were defined as days with maximum daily averaged 8-h (MDA8) concentrations over North China larger than 160 μg m^{-3}, and OPEs were defined as periods with 3 or more consecutive OPDs. Observations showed that there were 167 OPDs and 27 OPEs in North China during 2014-2017, in which 123 OPDs and 21 OPEs occurred in May-July. We found that OPEs in North China occurred under a typical weather pattern with high daily maximum temperature (Tmax), low relative humidity (RH), anomalous southerlies and divergence in the lower troposphere, an anomalous high-pressure system at 500 hPa and an anomalous downward air flow from 500 hPa to the surface. Under such a weather pattern, chemical production of O_3 was high between 800 and 900 hPa, which was then transported downward to enhance O_3 pollution at the surface. A standardized index I_OPE was defined by applying four key meteorological parameters, including Tmax, RH, meridional winds at 850 hPa (V850) and zonal winds at 500 hPa (U500). I_OPE can capture approximately 80-% of the observed OPDs and OPEs, which has implications for forecasting OPEs in North China.

1 Introduction

Ground-level ozone (O_3) is generated by photochemical reactions involving nitrogen oxides (NO_x) and volatile organic compounds (VOCs) (FinlaysonPitts and Pitts, 1997; Sillman, 1999). Enhanced surface O_3 concentrations increase premature mortality (e.g., Bell et al., 2006; Anenberg et al., 2010; Lelieveld et al., 2015; Nuvolone et al., 2018) and reduce crop yields (e.g., Fuhrer et al., 1997; Krupa et al., 1998; Ainsworth et al., 2012; Mills et al., 2018). O_3 pollution events (OPEs) occur frequently in megacities with sufficient O_3 precursors during summertime when solar radiation is strong (Solomon et al.,

2000; Wang et al., 2006a; Wang et al., 2006b; Roy et al., 2008; Carro-Calvo et al., 2017; Fix et al., 2018). As a result, the formation mechanisms of and prevention strategies for ground-level O_3 has been a focus in many countries around the world. Ozone concentrations are influenced by meteorological parameters. High temperature can change O_3 concentrations by accelerating O_3 chemical production rates and enhancing natural emissions such as biogenic emissions and NO_x from soil (Jacob and Winner, 2009). Blommer et al. (2009) analyzed observed O_3 from 1987 to 2007 across the rural eastern US and showed that as temperature increased by 1 K, O_3 concentrations increased by an average of 3.2 ppbv prior to 2002 but increased by an average of 2.2 ppbv after 2002 because of the reduction in anthropogenic NO_x emissions. Rasmussen et al. (2012) used observed O_3 and temperature in the eastern US during 1988-2009 to characterize the sensitivity of summer time O_3 to temperature. These authors showed that the sensitivities were 3-6 ppbv K^{-1} over the northeast, 3-4 ppbv K^{-1} over the Great Lakes, and 3-6 ppbv K^{-1} over the Middle Atlantic states. Relative humidity (RH) is also found to be an important parameter for O_3 formation. Zhang et al. (2015) showed that values of RH for days with top 10% O_3 concentrations were lower compared to those for days with bottom 10% O_3 concentrations by examining continuous observations of O_3 and meteorological parameters in Guangzhou during March 2013 to February 2014.~~Zhang et al. (2015) showed that days with the highest 10 % O_3 concentrations were associated with lower RH than days with the lowest 10 % O_3 concentrations in Guangzhou by examining continuous observations of O_3 and meteorological parameters during March 2013 to February 2014.~~ Kavassalis and Murphy (2017) reported a negative correlation between summer-time O_3 concentrations and RH on the basis of observed O_3 and RH from 1987 to 2015 at 101 rural sites in the US. Moreover, cloud fraction influences O_3 concentrations by changing the near-surface solar radiation and hence photochemical reaction rates. Jeong and Park (2013) showed, by using a 3-D global chemical and transport model (GEOS-Chem), that the increases in O_3 concentration in East Asia from 1985-1989 to 2002-2006 could be explained in part by the decreases in cloud cover.

In addition to the local meteorological parameters, O_3 concentrations are also influenced dynamically by large-scale circulations. By analyzing 11 years of ozonesonde data, Zhou et al. (2013) showed that the interannual variability of O_3 over Hong Kong was closely associated with the East Asian monsoon; circulations during monsoon season influence the transport of continental pollutants to Hong Kong. By using the GEOS-Chem model, Yang et al. (2014) examined the interannual variation of summertime O_3 and found a positive correlation between the strength of the East Asian summer monsoon and summertime O_3 concentration averaged over China because of the monsoon-driven variations in transboundary transport. Liao et al. (2017) carried out composite analysis on observed surface O_3 concentrations in the Yangtze River Delta (YRD) during 2013-2016 for ten typical circulation types identified by the automated Lamb weather type approach (Jenkinson and Collison, 1977). These authors found that O_3 concentrations in the YRD were high under the influence of westerlies, which occur frequently in summer associated with the subtropical high. Under such conditions, high temperatures and strong solar radiation in the YRD, together with the transport of biogenic VOCs from the mountain areas of Anhui and Zhejiang provinces, led to high O_3 levels in the YRD. Zhao and Wang (2017) reported that the daily variability of West Pacific subtropical high (WPSH) can influence the daily variability of surface-layer O_3 over eastern China in summer of 2014-2016. They found, by using observed O_3 and reanalyzed data, that O_3 concentrations decreased in South China and increased in

North China during days with a high WPSH-I index, which is an indicator of the intensity of WPSH at the 500 hPa level. A strong WPSH leads to moist, cloudy weather and low temperatures in South China and dry, sunny weather in North China. Previous studies also reported that OPEs are influenced by meteorological conditions. Zhang et al. (2017), utilizing 30 years of O_3 observations and meteorological variables over the US, showed that O_3 extreme days (location-specific 95th percentile) overlapped with 32-% of temperature extreme days, along with low RH and low wind speed. By using both observations and a regional chemistry-climate model, Pu et al. (2017) showed that a heat wave event in YRD during the summer of 2013 led to a severe O_3 pollution episode with a peak O_3 concentration of 160.5 ppbv as a result of the accelerated chemical reaction, low cloud fraction and stagnant conditions. By using the GEOS-Chem model and observed O_3 concentrations, Zhang and Wang (2016) showed that extreme drought events also led to three high O_3 episodes (with peak concentrations of 70 ppbv) in October 2010 in the southeast US by the enhanced emissions of biogenic isoprene from water-stressed plants. Moreover, regional transport of O_3 and precursors (such as NO_x mand isoprene) are important for OPEs. For example, Whaley et al. (2015) used the GEOS-Chem model with tagged-O_3 to identify the sources of O_3 for 15 OPEs in Toronto during 2004-2007 and found that O_3 in the northeast US contributed 26-% to O_3 in Toronto during OPEs. They also used the GEOS-Chem adjoint model to examine the sensitivities of O_3 concentrations during OPEs in Toronto to emissions of precursors in different regions and found a strong sensitivity to the southern Ontario and US fossil fuel NO_x emissions and natural isoprene emissions. Currently, previous studies on OPEs in China were focused on one single observational site or a few episodes (e.g., Wang et al., 2006c; Shen et al., 2015; Li et al., 2017a), and few studies have systematically examined OPEs in a regional scope, especially for North China (36.5°N-40.5°N, 114.5°E-119.5°E), where the highest O_3 peak concentrations were observed (Wang et al., 2017).

The scientific goals of this work are as follows: (1) to characterize the frequencies and intensities of OPEs in North China, (2) to identify key meteorological parameters that can be used to define a typical weather pattern for OPEs in North China, and (3) to quantify the contributions of different chemical and physical processes to OPEs under such a typical weather pattern. The integrated process rate (IPR) analysis is a widely used method to quantify the contributions of different processes to O_3 (Goncalves et al., 2009; Jiang et al., 2012; Li et al., 2012). In Sect. 2, observed O_3 concentrations, reanalyzed meteorological data, a model description, and the IPR analysis method are briefly introduced. Section 3 presents the observed frequency and intensity of OPEs in North China during 2014 to 2017.~~Section 3 presents the observed and spatiotemporal distributions of OPEs in North China during 2014 to 2017.~~ Section 4 describes the key meteorological parameters that lead to OPEs and the definition of a standardized index to represent a typical weather pattern for OPEs. Section 5 examines how the typical weather pattern leads to OPEs by IPR analysis in the GEOS-Chem model.

2 Methods

2.1 Observed ground-level O_3 concentrations

The ground-level hourly O_3 concentrations are obtained from the national air quality monitoring network of China (http://datacenter.mee.gov.cn/websjzx/queryIndex.vm~~http://datacenter.mep.gov.cn/websjzx/queryIndex.vm~~), which was established in 2012 by the Ministry of Environment Protection of China. O_3 concentrations from this network have units of μg m^{-3}. Under the condition of 25°C and 1013.25 hPa, 1 μg m^{-3} of O_3 is approximately 0.5 ppbv. Hourly O_3 concentrations are available at 1582 sites during 2014-2017. For each site, the maximum daily 8-h average concentration (MDA8) of O_3 is calculated by utilizing an 8-h moving average window for each day. To ensure the data quality, the 8-h moving window has to contain more than 6-h valid observations, and the number of days with valid O_3 MDA8 has to be more than 15 for each month. As a result, 740 among the 1582 sites in China (62 sites among the 101 sites in North China (36.5°-40.5°N, 114.5°-119.5°E), Fig. S1~~67 sites among the 114 sites in North China (36°-40.5°N, 114.5°-119.5°E)~~) are selected and used in this study. The spatial distribution of these selected sites and the region of North China are shown in Fig. 1.

The China National Ambient Air Quality Standard (GB3095-2012) states that O_3 concentration exceeds the national air quality standard if the MDA8 O_3 concentration of a location is higher than 160 μg m^{-3}. In this study, we aim to investigate O_3 pollution over a large area rather than at a single site; we define O_3 polluted days in North China as the days with MDA8 O_3 concentrations averaged over North China exceeding 160 μg m^{-3}. We also define an ozone episode in North China as three or more consecutive days of regional O_3 pollution.

2.2 Reanalyzed meteorological fields

Meteorological fields are taken from Version 2 of Modern Era Retrospective-analysis for Research and Application (MERRA2), which was generated from the NASA Global Modeling and Assimilation Office (GMAO) by using Version 5 data assimilation system (DAS) of the Goddard Earth Observing System Model. Compared with the first version of MERRA, MERRA2 has assimilated more observations and made many improvements and updates in DAS. The original MERRA2 data has a horizontal resolution of 0.5° latitude x 0.625° longitude and 72 vertical layers (Molod et al., 2015). The GEOS-Chem model has the same horizontal resolution over the nested domain but the GEOS-Chem support team has lumped the 72 vertical layers into 47 layers to save computational resources. The lumped vertical levels are within the 32th model layer (about 190 hPa) and the top of atmosphere (about 0.01 hPa). ~~(Molod et al., 2015). The MERRA2 reanalyzed meteorological dataset in the Extended Asia domain (11°S-55°N, 60°E-150°E) has a horizontal resolution of 0.5° latitude × 0.667° longitude and 47 vertical layers up to 0.01 hPa.~~ The temporal resolution for surface meteorological parameters (such as 2-meter air temperature) is 1 h and that for atmospheric meteorological parameters (such as relative humidity and wind) is 3 h. To investigate the key meteorological factors that lead to OPEs, daily maximum 2-meter temperature (Tmax), daily mean relative humidity (RH) at the surface, daily averaged meridional and zonal winds at 850 hPa and 500 hPa (U850, V850, U500 and V500, where westerlies and southerlies have positive values) during 2014-2017 are utilized. In addition, due to the

lack of geopotential heights in the MERRA2 dataset, daily mean geopotential heights at 850 hPa and 500 hPa from the National Center for Environmental Prediction (NCEP) and National Center for Atmospheric Research (NCAR) global reanalysis at a resolution of 2.5° latitude by 2.5° longitude are utilized. The daily time series of a meteorological parameter x at a specific model grid cell over May to July of 2014-2017 is standardized by:

$$[x_i] = \frac{x_i - \frac{\sum_i^n x_i}{n}}{s_i} \quad (1)$$

where x_i indicates the parameter x on day i, n is the total number of days over May to July in 2014-2017, s_i indicates the standard deviation of the daily time series. $[x_i]$ is the standardized anomaly for parameter x on day i. ~~All the time series of meteorological parameters have been detrended first and then standardized by their respective standard deviation to remove interannual or seasonal variability.~~

2.3 GEOS-Chem model

The hourly O_3 concentrations from May to July for 2014-2017 are simulated by the nested version of the 3-D global chemical transport model (GEOS-Chem, version 11-01) driven by the MERRA2 reanalysis meteorological data. Over the nested domain (11°S-55°N, 60°E-150°E), the model resolution is the same as that of the MERRA2 dataset, as described above. Concentrations of all tracers in lateral boundaries are provided by the global GEOS-Chem simulation with 2° latitude ×2.5° longitude horizontal resolution.

The GEOS-Chem model employs a fully coupled NO_x-O_x-hydrocarbon-aerosol chemistry mechanism (Bey et al., 2001; Park et al., 2003; Pye et al., 2009) to simulate concentrations of gas-phase pollutants (such as NO_x and O_3) and aerosols (including sulfate, nitrate, ammonium, OC and BC, sea salt, and mineral dust). The LINOZ scheme is used for stratospheric O_3 chemistry (McLinden et al., 2000). The vertical mixing in planetary boundary layers (PBL) is calculated by a nonlocal scheme (Lin and McElroy, 2010). The anthropogenic emissions of CO, SO_2, NO_x, NH_3 and VOCs in the simulated domain are obtained from MEIC emission inventory, which includes emissions from industry, power, residential and transportation sectors from 2014 to 2017 (Li et al., 2017b; Zheng et al., 2018). The biogenic emissions in GEOS-Chem employ the MEGAN v2.1 biogenic emissions with updates from Guenther et al. (2012).

2.4 IPR analysis method

Five major processes that influence O_3 concentrations include net chemical production, horizontal advection, vertical advection, dry deposition, and diffusion (vertical PBL mixing process in GEOS-Chem model). Integrated process rate (IPR) analysis is used to evaluate the daily relative contributions of individual processes to an OPE in the studied domain by using the following formula (Goncalves et al., 2009):

$$PC_i(\%) = \frac{PC_i}{\sum_i^n abs(PC_i)} \times 100\ \%, \quad (~~1~~2)$$

where PC_i is the percentage contribution of process i to O_3 mass in the specific domain and $abs(PC_i)$ is the absolute value of PC_i. n is the total number of processes (n is 5 in our analysis). $PC_i(\%)$ is the relative contribution of process i to O_3 mass. It is noted that the sum of process contributions ($PC_i(\%)$) is not 100-%, but the sum of the absolute values of $PC_i(\%)$ equals 100–%. The IPR analysis method has been applied to identify the key processes contributing to extreme air pollution episodes as well as the interannual and decadal variations (Mu and Liao, 2014; Lou et al., 2015; Shu et al., 2016).

3 Frequencies and intensities of OPEs in North China

3.1 Spatiotemporal distributions of surface layer O_3

Figure 1 shows the monthly mean MDA8 O_3 concentrations averaged over 2014-2017 at the 740 observational sites. The MDA8 O_3 values show obvious seasonal variations in eastern China. The monthly mean MDA8 O_3 values at most sites in eastern China were lower than 100 μg m^{-3} during November to March, while the values were generally high during April-October, especially in North China and the YRD region. North China had the highest MDA8 O_3 concentrations from May to July. In June, the most polluted month, the MDA8 O_3 concentrations at 40 % (25/62) of observational sites in North China exceeded 160 μg m^{-3}, in which four sites (two sites in Baoding, one in Hengshui and the other in Zibo) even exceeded 180 μg m^{-3}.

Figure 2a shows the seasonal and interannual variations in MDA8 O_3 concentrations averaged over all 62 sites in North China. The MDA8 O_3 concentrations in North China peaked in June and had relatively high values from May to July. In 2016 and 2017, a secondary peak of concentration showed up in September, but it is difficult to conclude whether this was a general or accidental feature with the limited four years of data. With respect to the interannual variation, MDA8 O_3 concentrations in most months exhibited an increasing trend from 2014 to 2017. The MDA8 O_3 concentration over North China reached the highest value of 182 μg m^{-3} in June of 2017. This increasing trend indicates that the strict emission reduction measures in China in recent years had little effect on O_3 pollution in North China.

3.2 Ozone polluted days and the frequency of OPEs

Figure 2b shows the O_3 polluted days in North China (the days with an average MDA8 O_3 concentration over North China exceeding 160 μg m^{-3}) in different months of 2014-2017. From 2014 to 2017, there were 167 O_3 polluted days in North China, in which 123 days (70-%) occurred in the months of May to July. In 2014, July and August had the highest number of O_3 polluted days (10 days). In 2015-2017, the number of O_3 polluted days was the highest in June and kept increasing. Ozone polluted days in North China had values of 11, 16 and 20 days in June of 2015, 2016, and 2017, respectively.

Figure 2c shows the number of OPEs in North China in each month of 2014-2017. An O_3 pollution event in North China is defined as three or more consecutive days of O_3 pollution. There were 27 OPEs in the studied time period, and 21 of these OPEs occurred in May to July. Except for June of 2014, North China suffered 1–3 OPEs per month in May to July of 2014-

2017. As shown above, O_3 pollution in North China was the worst in May to July. The 21 OPEs in these three months of 2014-2017 are further analyzed in the following sections.

3.3 Intensities of OPEs in North China

Figure 3 shows the mean and maximum MDA8 O_3 concentrations as well as the duration of 21 OPEs over May to July in the years of 2014-2017 in North China. The averaged MDA8 O_3 concentration for OPEs is 193.0 μg m^{-3}, indicating high intensities of OPEs. The maximum MDA8 O_3 concentrations for a single day during OPEs can even reach 243.8 μg m^{-3}, and over half of the episodes (11/21) have at least one day where MDA8 O_3 concentrations exceed 200 μg m^{-3}. Moreover, OPEs last for many consecutive days. The mean duration of OPEs is 4.3 days, while some episodes can last for one week and even longer (e.g., the episodes starting from June 16th, 2016 and June 14th, 2017). Understanding the kind of weather pattern that leads to these long-lasting OPEs with high O_3 concentrations is quite necessary.

4 A Typical weather pattern for OPEs

4.1 Composited weather pattern for OPEs

Figure 4 shows the composited weather pattern for 21 OPEs identified in North China (36.5°N-40.5°N, 114.5°E-119.5°E) during May to July of 2014-2017. We examine the composited Tmax, RH, winds and SLP at the surface, winds and geopotential height at 850 hPa, winds and geopotential height at 500 hPa, vertical pressure velocity and divergence. All these daily parameters in May to July of 2014-2017 are standardized by utilizing Eq. (1). ~~All these daily parameters in May to July of 2014-2017 are detrended first to remove interannual or seasonal variability. Then, for each parameter, we calculate the standardized anomalies by using the following formula:~~

~~$$[x_{i,d}] = \frac{x_{i,d} - \overline{x_i}}{s_i} \quad (2)$$~~

~~where $x_{i,d}$ indicates the detrended value for parameter i on day. $\overline{x_i}$ and s_i indicate the mean value and the standard deviation of the detrended daily time series for parameter i, respectively. $[x_{i,d}]$ is the standardized anomaly for parameter i on day d.~~ During OPEs, positive Tmax anomalies (Fig. 4d) and negative RH anomalies (Fig. 4e) occur in North China, indicating hot and dry weather conditions at the surface. The wind and pressure fields show a similar pattern at the surface (Fig. 4c) and at 850 hPa (Fig. 4b). Anomalous southerlies prevail in North China, accompanied by anomalous high pressure in the east and anomalous low pressure in the west. At the 500 hPa altitude, North China is under the influence of an anomalous anti-cyclone (high pressure) (Fig. 4a), which causes high temperature and low RH at the surface.

The composited pressure-latitude cross-sections of vertical velocity and divergence for 21 OPEs from 1000 hPa to 500 hPa averaged over 114.5°E to 119.5°E, the west and east boundary of North China, are shown in Fig. 4f and 4g, respectively. Except for the north of 39°N under 850 hPa, North China shows a downward airflow anomaly from 1000 hPa to 500 hPa

during OPEs, which is a typical feature of the high-pressure system. In fact, the upward anomaly under 850 hPa in the northern domain is a fake signal because the elevation sharply increases to approximately 1000 m at Yan Mountain to the north of 39°N, which leads to the surface pressure being lower than 900 hPa (~1000 m) or even 850 hPa (~1500 m). As a result, the vertical velocity under 850 hPa for the reanalyzed dataset is unreliable to the north of 39°N. Figure 4g shows the divergence anomaly during OPEs in North China. Strong divergence occurs between 950 and 850 hPa. The anomalous downward flow transports air to the lower troposphere and leads to the anomalous divergence.

4.2 Correlations between meteorological parameters and O_3 concentrations

To identify the key meteorological factors associated with the MDA8 O_3 concentrations in North China, we examine the correlation coefficients between the MDA8 O_3 concentration averaged over North China and the meteorological parameters, including daily Tmax and daily mean RH, planetary boundary layer height (PBLH), surface level pressure (SLP), and meridional and zonal wind speed at 1000 hPa (U1000, V1000), 850 hPa (U850, V850) and 500 hPa (U500, V500). These parameters at each grid cell are ~~detrended first and then~~ standardized as described in Sect. ~~4.1~~2.2. Figure 5 shows the correlation coefficients between daily MDA8 O_3 concentration in North China and the ten standardized meteorological parameters. MDA8 O_3 concentrations in North China exhibit positive correlation with Tmax (Fig. 5a), PBLH (Fig. 5c), V1000 (Fig. 5f) and V850 (Fig. 5h) in the vicinity of North China and with U500 (Fig. 5i) in the north and V500 (Fig. 5j) in the west of North China. MDA8 O_3 in North China has a negative correlation with RH (Fig. 5b), SLP (Fig. 5d), U500 (Fig. 5i), and V500 (Fig. 5j). MDA8 O_3 is found to have a weak correlation with U1000 (Fig. 5e) and U850 (Fig. 5g). It should be noted that some meteorological factors are closely related. For instance, previous studies have revealed that PBLH is positively correlated with surface temperature (Zhang et al., 2013) but negatively correlated with SLP (Seidel et al., 2010; Guo et al., 2016). Winds at 1000 hPa and 850 hPa are usually highly correlated and show similar patterns. As a result, four meteorological factors are selected to represent the key meteorological conditions for high MDA8 O_3 concentrations: Tmax represents the thermal condition, RH indicates the humidity condition, 850 hPa ~~zonal~~ meridional winds indicate circulation in the lower atmosphere and 500 hPa ~~meridional~~ zonal winds describe the dominate large-scale circulation.

4.3 Definition of I_OPE

As described above, the weather pattern associated with high MDA8 O_3 concentrations in North China can be characterized by high Tmax and low RH at the surface, anomalous southerlies in the lower atmosphere, and anomalous high pressure at the 500 hPa level. We can then define an index I_OPE to represent such a weather pattern and to examine how many O_3 polluted days and OPEs in North China occurred under such a weather pattern. For a specific day, I_OPE is defined as follows:

$$I\_OPE = [\sum_x index\_x], \quad (3)$$

where x indicates Tmax, RH, V850 or U500, and the square bracket indicates standardization. The four index_x values are calculated by:

$$index\_Tmax = \left[\sum_{i,j}^{35°N-45°N,110°E-120°E} Tmax_{i,j}\right], \quad (4)$$

$$index\_RH = -\left[\sum_{i,j}^{35°N-45°N,110°E-120°E} RH_{i,j}\right], \quad (5)$$

$$index\_V850 = \left[\sum_{i,j}^{35°N-45°N,107°E-120°E} V850_{i,j}\right], \quad (6)$$

$$index\_U500 = \left[\sum_{i,j}^{45°N-55°N,105°E-125°E} U500_{i,j}\right] - \left[\sum_{i,j}^{34°N-40°N,105°E-125°E} U500_{i,j}\right], \quad (7)$$

where *i* and *j* indicate latitude and longitude of the grid cell, respectively. $Tmax_{i,j}$, for example, is the Tmax in grid (*i, j*) on a specific day after the time series is ~~detrended and~~ standardized, as described in Sect. ~~4.1~~2.2. Domains with strong correlation between each parameter (Tmax, RH, V850, or U500) and MDA8 O_3 concentrations in North China are shown in Fig. 5 by red rectangles. Since RH exhibits a negative correlation with MDA8 O_3 concentrations, index_RH has a negative sign in Eq. (5).

Figure 6 shows the time series of MDA8 O_3 concentrations in North China and the five indexes (index_Tmax, index_RH, index_V850, index_U500 and I_OPE). The OPEs in Fig. 6a (pink rectangles) are captured by the five indexes. Among all the indexes, index_Tmax has the strongest correlation with MDA8 O_3 concentrations, with a correlation coefficient (*r*) of ~~0.52~~0.56. The correlation coefficients between index_RH, index_V850 and index_U500 and MDA8 O_3 concentrations are ~~0.32~~0.30, ~~0.35~~0.37, and ~~0.41~~0.44, respectively. It is interesting that the correlation coefficient between I_OPE and MDA8 O_3 is ~~0.64~~0.67, which is higher than that between each individual index and MDA8 O_3, indicating that MDA8 O_3 concentrations in North China are influenced by multiple meteorological factors rather than a single factor.

Figure ~~7~~ S2 shows the composite patterns of anomalies of meteorological fields (Tmax at the surface, RH at the surface, winds at 850 hPa, and winds at 500 hPa) for OPEs (Fig. ~~7a~~S2 a-d) and for days with I_OPE >0 (Fig. ~~7e~~S2 e-h). The similarity in patterns between these two types of composite analyses indicates that I_OPE can capture the weather pattern associated with OPEs, including the high Tmax, low RH, anomalous southerlies at 850 hPa, and the anomalous anti-cyclonic winds at 500 hPa. From May to July over 2014-2017, there were 123 days with regionally averaged observed O_3 concentrations of greater than 160 μg m^{-3}, in which ~~82.1~~83.7 % days (~~101~~103/123) occurred under the condition of I_OPE>0. Conversely, ~~54.3~~55.0 % days (~~101~~103/186) with I_OPE>0 and ~~72.5~~75.0 % days (~~37/51~~42/56) with I_OPE>1 were observed for O_3 pollution days in North China. Among the observed 21 OPEs (90 days), 17 OPEs (~~69~~ 71 days) occurred under a weather pattern with I_OPE>0. Therefore, I_OPE can be used as a meteorological predictor for OPEs in North China.

5 Simulated OPEs and IPR analysis

5.1 Simulated OPEs

We have identified a typical weather pattern associated with OPEs in North China, as presented in Sect. 4. Here, we use the GEOS-Chem simulation of O_3 in May-July of 2014-2017 to quantify the contributions of different chemical and physical

processes to OPEs under such a weather pattern. Figure ~~8~~ 7 shows the time series of observed and simulated daily MDA8 O_3 averaged over North China. The correlation coefficients between the observed and simulated MDA8 O_3 are 0.53, 0.64, 0.61, and 0.71 in 2014, 2015, 2016, and 2017, respectively, indicating that the GEOS-Chem model can simulate the daily variation in MDA8 O_3. Compared to observed MDA8 O_3 concentrations, the simulated concentrations have a mean bias (MB) (normalized mean bias (NMB)) of 2.4 μg m^{-3} (1.7~~-~~%) in 2014, 6.7 μg m^{-3} (4.9~~-~~%) in 2015, 1.8 μg m^{-3} (1.2~~-~~%) in 2016, and -12.5 μg m^{-3} (-8.4~~-~~%) in 2017. For all the data samples in May-July of 2014-2017, the observed MDA8 O_3 concentration averaged over North China is 146.8 μg m^{-3}, and the simulated mean value is also 146.8 μg m^{-3}. The linear regression by the least squares method through the origin between observed and simulated MDA8 O_3 has a regression coefficient of 0.96 (Fig. S3), indicating the capability of the model in simulating the MDA8 O_3 concentrations.~~The linear regression through the origin between observed and simulated MDA8 O_3 has a regression coefficient of 0.96, indicating the capability of the model in simulating the MDA8 O_3 concentrations.~~

The GEOS-Chem model, however, has some difficulties in capturing the peak values of MDA8 O_3, as reported in previous studies by Zhang and Wang (2016) and Ni et al. (2018). During May-July of 2014-2017, for the O_3 polluted days with observed MDA8 O_3 > 160 μg m^{-3}, comparisons of simulated values with observations show an NMB of -14.6~~-~~%. As a result, if the same threshold (160 μg m^{-3}) is applied in the model to define O_3 polluted days, only ~~8~~ 9 OPEs (highlighted by pink rectangles in Fig. ~~8~~7) among the 17 OPEs with I_OPE>0 can be captured by the model. Considering that the model has an NMB of -14.6-% for the days with observed MDA8 O_3 > 160 μg m^{-3}, a revised lower threshold of 136.6 μg m^{-3} (160*85.4-%) is adopted to define the O_3 polluted days in the model, and consequently, 6 more OPEs are identified (highlighted by light blue rectangles in Fig. ~~8~~7). Therefore, among the 17 OPEs (~~69~~ 71 days) under the typical weather pattern, ~~14~~ 15 episodes (~~59~~ 63 days) can be identified by the model. We then carry out IPR analysis for these ~~14~~ 15 episodes (~~59~~ 63 days) to understand how the typical weather pattern leads to OPEs in North China.

5.2 IPR analysis

The vertical profile of simulated daily O_3 concentrations averaged over May to July in 2014-2017 as well as that composited over the 15 OPEs are shown in Fig. 8a. For both profiles, the O_3 concentrations are highest between 950 hPa and 850 hPa and are relatively lower at the surface due to the titration by high NO_x concentrations. When OPEs occur, O_3 concentrations are higher from the surface to 700 hPa (about 3 km altitude) but change little above 700 hPa, indicating that the enhancement of O_3 concentrations during OPEs occurs not only at the surface but also in and above the boundary layer.

Five processes that influence O_3 concentrations are analyzed, including net chemical production, horizontal advection, vertical advection, dry deposition, and diffusion. Note that wet deposition is not considered because of its small contribution to O_3 budget (Mickley et al., 1999; Liao et al., 2006). All of the processes are diagnosed at every time step and then summed over each day in the simulation. To avoid the discrepancy in O_3 budget because of different lasting days of OPEs, the daily mean ~~O_3 mass flux (MF (Gg O_3 day^{-1}))~~net change in O_3 mass (Gg O_3 day^{-1}) is presented for each process. We also calculate PC(%), as described in Sect. 2.4, to examine the relative percentage contribution of each process. The horizontal domain for

the IPR analysis is North China (36.5°N-40.5°N, 114.5°E-119.5°E). We diagnose first the vertical profiles of net changes in O_3 massMF for the model layers from the surface to 500 hPa averaged over all days in May-July of 2014-2017 and then quantify the anomalies inanomalous net changes in O_3 massMF during OPEs relative to the seasonal mean flux to identify the major changes in processes that lead to high O_3 episodes. Finally, mechanisms that lead to OPEs in North China are discussed on the basis of process analysis.

5.2.1 Vertical profiles of net changes in O_3 massMF averaged over May-July of 2014-2017

Figure 9a 8b shows the vertical profiles of net changes in O_3 massMF for each process over North China averaged over all days in May-July of 2014-2017. Note that the MF of each process at a specific level indicates the net O_3 mass change within this level rather than the flux across this level, especially for the vertical processes such as diffusion and vertical advection.

Net chemical production at the surface is a large negative value (-2.5 Gg O_3 day^{-1}) (Fig. 9a8b) as a result of the O_3 titration effect by high NO_x concentrations at the surface. In the upper layers, because of the decreases in NO_x concentrations and the stronger radiations, net chemical production has positive contributions to O_3 concentration over North China, with high values exceeding 1.4 Gg O_3 day^{-1} at approximately 900 hPa and 800 hPa. Note that net chemical production is practically the only process that increases O_3 between 930 hPa and 800 hPa. Above 750 hPa, net chemical production decreases due to the decreases in O_3 precursors.

Diffusion process in GEOS-Chem model describes the mixing in the boundary layer, which transports O_3 along the concentration gradient. Since O_3 concentrations are higher at 950 hPa to 850 hPa than at the surface (Fig. 8a), the diffusion transports O_3 from the upper boundary layer downwardly to the surface. As a result, the IPR analysis shows that the net mass change in O_3 by diffusion is negative between 950 and 850 hPa but positive at the surface (Fig. 8b). Note that the net changes in O_3 mass over North China by diffusion process should approximately equal to zero (Table 1) if we integrate the change in O_3 mass by diffusion from the surface to 850 hPa because diffusion is an internal vertical transport. The downward transport of O_3 by diffusion was also reported in previous IPR analyses (e.g., Khiem et al., 2010; Li et al., 2012; Tang et al., 2017).

Diffusion is a process that mainly occurs in the boundary layer, which transports O_3 along the concentration gradient and mixes O_3 evenly. The sum of the mass fluxes of diffusion from the surface to 850 hPa is small (0.36 Gg O_3 day^{-1}), indicating that diffusion has a small effect on the total mass of O_3 in the boundary layer. However, the diffusion process is important in the boundary layer, which has negative contributions between 950 and 800 hPa but a positive contribution at the surface (Fig. 9a). Since the mass flux of diffusion for the whole boundary layer is small, it is indicated that O_3 aloft is transported downward to be mixed at the surface by the diffusion process. Such downward transport and mixing of O_3 were also reported in previous IPR analyses (e.g., Khiem et al., 2010; Li et al., 2012; Tang et al., 2017).

Vertical advection exhibits negative net changes in O_3 massMF values from the surface to approximately 750 hPa and then becomes positive in the upper layers (Fig. 9a8b), indicating that O_3 is transported from the lower to upper atmosphere by vertical advection under the seasonal mean condition. Horizontal advection increases O_3 from the surface to approximately

900 hPa but decreases O_3 at the upper levels (Fig. ~~9a~~8b). Dry deposition occurs at the surface and has a~~n~~ net change in O_3 mass~~MF~~ of -4.9 Gg O_3 day^{-1} under the seasonal mean condition.

5.2.2 Comparison of processes during OPEs with the seasonal mean values

Figure ~~9b~~ 8c shows the profiles of the anomaly of each process during OPEs relative to the seasonal mean value over May-July of 2014-2017. During OPEs, net chemical production at layers from the surface to approximately 800 hPa is enhanced significantly, generating O_3 in North China. The largest enhancement occurs between 950 hPa and 800 hPa, exceeding +0.3 Gg O_3 day^{-1}. With respect to diffusion during OPEs, both the positive contribution at the surface and the negative contributions in the upper layers increase (Fig. ~~9b~~8c), indicating that more O_3 is mixed from the upper levels to the surface to increase the surface O_3 concentration during OPEs.

The vertical and horizontal advections during OPEs are the processes that have the largest changes relative to the mean condition. Anomalous vertical advection increases O_3 from the surface to approximately 800 hPa but decreases O_3 above 700 hPa. A large amount of O_3 is transported from aloft to the lower atmosphere by vertical advection, which will be examined in detail in Sect. 5.2.3 below. Horizontal advection reduces O_3 from the surface to approximately 800 hPa, which will also be explained in Sect. 5.2.3.

Since O_3 concentrations at the surface are determined by the processes in the boundary layer, we show in Table 1 the seasonal mean net changes in O_3 mass~~MF~~, the absolute net changes in O_3 mass~~MF~~ during OPEs, and their difference for each process in the boundary layer (from the surface to 850 hPa) over North China. Relative to the mean condition, net chemical production, diffusion, dry deposition, horizontal advection, and vertical advection during OPEs change by 3.3, -1.1, -0.4, -9.1 and 8.1~~3.3, -1.2, -0.4, -11.4, and 10.4~~ Gg O_3 day^{-1}, indicating that net chemical production~~, horizontal advection~~ and vertical advection are the most dominant processes that lead to OPEs. During OPEs, net chemical production and vertical advection increase O_3 in North China, while horizontal advection reduces O_3 in this region.

5.2.3 Mechanisms for the typical weather pattern leading to OPEs

The typical weather pattern for OPEs in North China has been identified in Sect. 4, which is characterized by hot and dry air at the surface, anomalous southerlies and divergence in the lower troposphere, anomalous high pressure at 500 hPa and anomalous downward airflows from 500 hPa to the surface. The hot and dry air under the high-pressure system accelerates chemical production of O_3 in and above the boundary layer (e.g., Zhang and Wang, 2016; Pu et al., 2017). Moreover, hot and sunny weather during OPEs increases the vertical concentration gradient (stronger chemical production at and above the upper boundary layer), leading to more O_3 transported downward to the surface as described in Sect. 5.2.2.~~Moreover, the hot air is beneficial for developing the mixed layer, leading to more O_3 mixed downward to the surface during OPEs, as described in Sect. 5.2.2.~~

The diagnosed vertical advection anomaly during OPEs can be explained by Fig. ~~10a~~9a, which shows the pressure-latitude cross-section of simulated daily mean O_3 concentrations as well as the anomalous vertical pressure velocity profile averaged

over North China during OPEs. Note that the regional mean vertical velocity near the surface is interfered by the Yan Mountain, as described in Sect. 4.1, so we will not discuss the vertical air flow below 950 hPa. The anomalous downward air flow is high at 850 hPa, and the net chemical production of O_3 is still strong above 850 hPa (Fig. ~~9b~~8c), leading to the large transport of O_3 to the boundary layer to form OPEs (Table 1).

Figures ~~10b~~9b-d show the anomalous winds and the simulated daily mean O_3 concentrations at 850 hPa, 950 hPa and the surface, respectively. The patterns of wind anomalies are similar at these three levels, all of which show a divergence of winds over North China, and anomalous southerlies prevail in this region. The divergence is caused by a high-pressure system at 500 hPa and is represented by index_U500 in the definition of I_OPE. Because O_3 concentrations in North China are the highest during OPEs, horizontal advection associated with the divergence has an effect of decreasing O_3 concentration in North China, as shown by the IPR analysis.

Currently, among the four indexes that are utilized to define I_OPE, the mechanisms for three of them (index_Tmax, index_RH and index_U500) have been demonstrated. It is of interest to understand the role of index_V850. On the one hand, the anomalous southerlies are associated with the high-pressure system. As Fig. 4b and Fig. 5h show, the strongest southerly anomalies at 850 hPa during OPEs are presented in the west of North China, which is consistent with the southerlies at the west boundary of the anti-cyclone circulation at 500 hPa. On the other hand, the southerlies are likely to have an effect of increasing the O_3 concentrations by transporting O_3 during OPEs. Figure ~~11~~10 presents the composite daily mean O_3 concentrations and winds at the surface, 950 hPa and 850 hPa for the first day and the last day of the OPEs. In the composited first day of the OPEs, O_3 concentrations in the south of North China are high (Fig. ~~11a~~10a-c). However, when the episodes are ending, O_3 concentrations decrease in the south domain but increase in North China (Fig. ~~11d~~10d-f), indicating that the O_3 transport strengthens OPEs with the southerly winds.

6 Conclusions

In this study, we utilized ground-level observations, reanalyzed meteorological data and a 3-D global transport and chemical model (GEOS-Chem) to understand the ozone pollution events (OPEs) over May-July of 2014-2017 in North China and their relationships with the weather pattern. O_3 polluted days in North China are defined as days with an average MDA8 O_3 concentration exceeding 160 μg m^{-3}, and OPEs are defined as episodes where O_3 pollution lasts for three days or longer.

Ground-based observations showed that North China had the worst O_3 pollution in China. There were 167 O_3 polluted days and 27 OPEs in North China in the years of 2014-2017, in which 123 O_3 polluted days and 21 OPEs occurred in May-July. The mean MDA8 O_3 concentrations for OPEs in May to July were 193.0 μg m^{-3}.

A typical weather pattern was identified for OPEs in North China in May–July (Fig. 11), which is characterized by high Tmax and low RH at the surface, anomalous southerlies and divergence in the lower troposphere, an anomalous high-pressure system at 500 hPa, and downward air flow from 500 hPa to the surface. The hot and dry air accelerates chemical production of O_3 in and above the boundary layer. The anomalous downward air flow under the high-pressure system

transports O_3 formed in the upper layers to the boundary layer. The anomalous southerlies associated with the high-pressure system transport O_3 from the south to North China, enhancing the intensity of OPEs. Four parameters, including Tmax, RH, V850 and U500, were selected to define a standardized index I_OPE to represent such a weather pattern. In May-July of 2014-2017, 83.7% (103/123)~~82 % (101/123)~~ of O_3 polluted days and ~~81~~ 80.9% (17/21) of OPEs occurred with I_OPE>0, indicating that I_OPE has the potential to be used for forecasting OPEs in North China.

Integrated process rate (IPR) analysis was applied in the GEOS-Chem model to quantify the contributions of each process (including net chemical production, diffusion, dry deposition, horizontal advection and vertical advection) to OPEs in North China. Relative to the mean condition, net chemical production, diffusion, dry deposition, horizontal advection, and vertical advection during OPEs change by 3.3, -1.1, -0.4, -9.1 and 8.1~~3.3, -1.2, -0.4, -11.4, and 10.4~~ Gg O_3 day^{-1}, indicating that net chemical production~~, horizontal advection,~~ and vertical advection are the most dominant processes that lead to OPEs. In North China, during OPEs, net chemical production has a high value at altitudes of 900 to 800 hPa and O_3 generated is transported downward to increase O_3 at the surface, whereas horizontal advection reduces surface O_3.

Data availability

The observed hourly ozone concentrations are derived from the Data Center of China's Ministry of Ecology and Environment (http://datacenter.mee.gov.cn/websjzx/queryIndex.vm~~http://datacenter.mep.gov.cn/websjzx/queryIndex.vm~~) over 2014-2017. The NCEP reanalyzed dataset is obtained from https://www.esrl.noaa.gov/psd/cgi-bin/data/getpage.pl. The GEOS-Chem model is an open-access model managed by the Atmospheric Chemistry Modeling group at Harvard University with support from institutes in North America, Europe, and Asia. The source codes, as well as the MERRA2 reanalyzed data, can be downloaded from http://acmg.seas.harvard.edu/geos/.

Author contribution

HL and CG conceived the study and designed the experiments. CG carried out the simulations and performed the analysis. CG and HL prepared the manuscript with contributions from all coauthors.

Competing interests

The authors declare that they have no conflict of interest.

Acknowledgements

This work was supported by the National Natural Science Foundation of China (under grants 91544219, 91744311, and 41475137) and by the Major Research Plan of National Social Science Foundation (under the grant of 18ZDA052). We

acknowledge the Data Center of China's Ministry of Ecology and Environment and NCAR teams for making their data publicly available. We acknowledge the efforts of the GEOS-Chem working groups for developing and managing the model.

References

Ainsworth, E. A., Yendrek, C. R., Sitch, S., Collins, W. J., and Emberson, L. D.: The Effects of Tropospheric Ozone on Net Primary Productivity and Implications for Climate Change, in: Annual Review of Plant Biology, Vol 63, edited by: Merchant, S. S., Annual Review of Plant Biology, 637-661, 2012.

Anenberg, S. C., Horowitz, L. W., Tong, D. Q., and West, J. J.: An Estimate of the Global Burden of Anthropogenic Ozone and Fine Particulate Matter on Premature Human Mortality Using Atmospheric Modeling, Environmental Health Perspectives, 118, 1189-1195, 10.1289/ehp.0901220, 2010.

Bell, M. L., Peng, R. D., and Dominici, F.: The exposure-response curve for ozone and risk of mortality and the adequacy of current ozone regulations, Environmental Health Perspectives, 114, 532-536, 10.1289/ehp.8816, 2006.

Bey, I., Jacob, D. J., Yantosca, R. M., Logan, J. A., Field, B. D., Fiore, A. M., Li, Q. B., Liu, H. G. Y., Mickley, L. J., and Schultz, M. G.: Global modeling of tropospheric chemistry with assimilated meteorology: Model description and evaluation, Journal of Geophysical Research-Atmospheres, 106, 23073-23095, 10.1029/2001jd000807, 2001.

Bloomer, B. J., Stehr, J. W., Piety, C. A., Salawitch, R. J., and Dickerson, R. R.: Observed relationships of ozone air pollution with temperature and emissions, Geophysical Research Letters, 36, 10.1029/2009gl037308, 2009.

Carro-Calvo, L., Ordonez, C., Garcia-Herrera, R., and Schnell, J. L.: Spatial clustering and meteorological drivers of summer ozone in Europe, Atmospheric Environment, 167, 496-510, 10.1016/j.atmosenv.2017.08.050, 2017.

FinlaysonPitts, B. J., and Pitts, J. N.: Tropospheric air pollution: Ozone, airborne toxics, polycyclic aromatic hydrocarbons, and particles, Science, 276, 1045-1052, 10.1126/science.276.5315.1045, 1997.

Fix, M. J., Cooley, D., Hodzic, A., Gilleland, E., Russell, B. T., Porter, W. C., and Pfister, G. G.: Observed and predicted sensitivities of extreme surface ozone to meteorological drivers in three US cities, Atmospheric Environment, 176, 292-300, 10.1016/j.atmosenv.2017.12.036, 2018.

Fuhrer, J., Skarby, L., and Ashmore, M. R.: Critical levels for ozone effects on vegetation in Europe, Environmental Pollution, 97, 91-106, 10.1016/s0269-7491(97)00067-5, 1997.

Goncalves, M., Jimenez-Guerrero, P., and Baldasano, J. M.: Contribution of atmospheric processes affecting the dynamics of air pollution in South-Western Europe during a typical summertime photochemical episode, Atmospheric Chemistry and Physics, 9, 849-864, 10.5194/acp-9-849-2009, 2009.

Guenther, A. B., Jiang, X., Heald, C. L., Sakulyanontvittaya, T., Duhl, T., Emmons, L. K., and Wang, X.: The Model of Emissions of Gases and Aerosols from Nature version 2.1 (MEGAN2.1): an extended and updated framework for modeling biogenic emissions, Geoscientific Model Development, 5, 1471-1492, 10.5194/gmd-5-1471-2012, 2012.

Guo, J., Miao, Y., Zhang, Y., Liu, H., Li, Z., Zhang, W., He, J., Lou, M., Yan, Y., Bian, L., and Zhai, P.: The climatology of planetary boundary layer height in China derived from radiosonde and reanalysis data, Atmospheric Chemistry and Physics, 16, 13309-13319, 10.5194/acp-16-13309-2016, 2016.

Jacob, D. J., and Winner, D. A.: Effect of climate change on air quality, Atmospheric Environment, 43, 51-63, 10.1016/j.atmosenv.2008.09.051, 2009.

Jenkinson, A.F., and Collison, F.P.: An initial climatology of gales over the North Sea. Synoptic Branch Memorandum No. 62. Met Office, Exeter. 1977.

Jeong, J. I., and Park, R. J.: Effects of the meteorological variability on regional air quality in East Asia, Atmospheric Environment, 69, 46-55, 10.1016/j.atmosenv.2012.11.061, 2013.

Jiang, F., Zhou, P., Liu, Q., Wang, T., Zhuang, B., and Wang, X.: Modeling tropospheric ozone formation over East China in springtime, Journal of Atmospheric Chemistry, 69, 303-319, 10.1007/s10874-012-9244-3, 2012.

Kavassalis, S. C., and Murphy, J. G.: Understanding ozone-meteorology correlations: A role for dry deposition, Geophysical Research Letters, 44, 2922-2931, 10.1002/2016gl071791, 2017.

Khiem, M., Ooka, R., Hayami, H., Yoshikado, H., Huang, H., and Kawamoto, Y.: Process analysis of ozone formation under different weather conditions over the Kanto region of Japan using the MM5/CMAQ modelling system, Atmospheric Environment, 44, 4463-4473, 10.1016/j.atmosenv.2010.07.038, 2010.

Krupa, S. V., Nosal, M., and Legge, A. H.: A numerical analysis of the combined open-top chamber data from the USA and Europe on ambient ozone and negative crop responses, Environmental Pollution, 101, 157-160, 10.1016/s0269-7491(98)00019-0, 1998.

Lelieveld, J., Evans, J. S., Fnais, M., Giannadaki, D., and Pozzer, A.: The contribution of outdoor air pollution sources to premature mortality on a global scale, Nature, 525, 367-+, 10.1038/nature15371, 2015.

Li, K., Chen, L., Ying, F., White, S. J., Jang, C., Wu, X., Gao, X., Hong, S., Shen, J., Azzi, M., and Cen, K.: Meteorological and chemical impacts on ozone formation: A case study in Hangzhou, China, Atmospheric Research, 196, 40-52, 10.1016/j.atmosres.2017.06.003, 2017a.

Li, L., Chen, C. H., Huang, C., Huang, H. Y., Zhang, G. F., Wang, Y. J., Wang, H. L., Lou, S. R., Qiao, L. P., Zhou, M., Chen, M. H., Chen, Y. R., Streets, D. G., Fu, J. S., and Jang, C. J.: Process analysis of regional ozone formation over the Yangtze River Delta, China using the Community Multi-scale Air Quality modeling system, Atmospheric Chemistry and Physics, 12, 10971-10987, 10.5194/acp-12-10971-2012, 2012.

Li, M., Zhang, Q., Kurokawa, J.-i., Woo, J.-H., He, K., Lu, Z., Ohara, T., Song, Y., Streets, D. G., Carmichael, G. R., Cheng, Y., Hong, C., Huo, H., Jiang, X., Kang, S., Liu, F., Su, H., and Zheng, B.: MIX: a mosaic Asian anthropogenic emission inventory under the international collaboration framework of the MICS-Asia and HTAP, Atmospheric Chemistry and Physics, 17, 935-963, 10.5194/acp-17-935-2017, 2017b.

Liao, H., Chen, W.-T., and Seinfeld, J. H.: Role of climate change in global predictions of future tropospheric ozone and aerosols, Journal of Geophysical Research-Atmospheres, 111, 10.1029/2005jd006852, 2006.

Liao, Z., Gao, M., Sun, J., and Fan, S.: The impact of synoptic circulation on air quality and pollution-related human health in the Yangtze River Delta region, Sci Total Environ, 607-608, 838-846, 10.1016/j.scitotenv.2017.07.031, 2017.

Lin, J.-T., and McElroy, M. B.: Impacts of boundary layer mixing on pollutant vertical profiles in the lower troposphere: Implications to satellite remote sensing, Atmospheric Environment, 44, 1726-1739, 10.1016/j.atmosenv.2010.02.009, 2010.

Lou, S., Liao, H., Yang, Y., and Mu, Q.: Simulation of the interannual variations of tropospheric ozone over China: Roles of variations in meteorological parameters and anthropogenic emissions, Atmospheric Environment, 122, 839-851, 10.1016/j.atmosenv.2015.08.081, 2015.

McLinden, C. A., Olsen, S. C., Hannegan, B., Wild, O., Prather, M. J., and Sundet, J.: Stratospheric ozone in 3-D models: A simple chemistry and the cross-tropopause flux, Journal of Geophysical Research-Atmospheres, 105, 14653-14665, 10.1029/2000jd900124, 2000.

Mickley, L. J., Murti, P. P., Jacob, D. J., Logan, J. A., Koch, D. M., and Rind, D.: Radiative forcing from tropospheric ozone calculated with a unified chemistry-climate model, Journal of Geophysical Research-Atmospheres, 104, 30153-30172, 10.1029/1999jd900439, 1999.

Mills, G., Sharps, K., Simpson, D., Pleijel, H., Broberg, M., Uddling, J., Jaramillo, F., Davies, W. J., Dentener, F., Van den Berg, M., Agrawal, M., Agrawal, S. B., Ainsworth, E. A., Buker, P., Emberson, L., Feng, Z., Harmens, H., Hayes, F., Kobayashi, K., Paoletti, E., and Van Dingenen, R.: Ozone pollution will compromise efforts to increase global wheat production, Global Change Biology, 24, 3560-3574, 10.1111/gcb.14157, 2018.

Molod, A., Takacs, L., Suarez, M., and Bacmeister, J.: Development of the GEOS-5 atmospheric general circulation model: evolution from MERRA to MERRA2, Geoscientific Model Development, 8, 1339-1356, 10.5194/gmd-8-1339-2015, 2015.

Mu, Q., and Liao, H.: Simulation of the interannual variations of aerosols in China: role of variations in meteorological parameters, Atmospheric Chemistry and Physics, 14, 9597-9612, 10.5194/acp-14-9597-2014, 2014.

Ni, R., Lin, J., Yan, Y., and Lin, W.: Foreign and domestic contributions to springtime ozone over China, Atmospheric Chemistry and Physics, 18, 11447-11469, 10.5194/acp-18-11447-2018, 2018.

Nuvolone, D., Petri, D., and Voller, F.: The effects of ozone on human health, Environmental Science and Pollution Research, 25, 8074-8088, 10.1007/s11356-017-9239-3, 2018.

Park, R. J., Jacob, D. J., Chin, M., and Martin, R. V.: Sources of carbonaceous aerosols over the United States and implications for natural visibility, Journal of Geophysical Research-Atmospheres, 108, 10.1029/2002jd003190, 2003.

Pu, X., Wang, T. J., Huang, X., Melas, D., Zanis, P., Papanastasiou, D. K., and Poupkou, A.: Enhanced surface ozone during the heat wave of 2013 in Yangtze River Delta region, China, Sci Total Environ, 603-604, 807-816, 10.1016/j.scitotenv.2017.03.056, 2017.

Pye, H. O. T., Liao, H., Wu, S., Mickley, L. J., Jacob, D. J., Henze, D. K., and Seinfeld, J. H.: Effect of changes in climate and emissions on future sulfate-nitrate-ammonium aerosol levels in the United States, Journal of Geophysical Research-Atmospheres, 114, 10.1029/2008jd010701, 2009.

Rasmussen, D. J., Fiore, A. M., Naik, V., Horowitz, L. W., McGinnis, S. J., and Schultz, M. G.: Surface ozone-temperature relationships in the eastern US: A monthly climatology for evaluating chemistry-climate models, Atmospheric Environment, 47, 142-153, 10.1016/j.atmosenv.2011.11.021, 2012.

Roy, S., Beig, G., and Jacob, D.: Seasonal distribution of ozone and its precursors over the tropical Indian region using regional chemistry-transport model, Journal of Geophysical Research-Atmospheres, 113, 10.1029/2007jd009712, 2008.

Seidel, D. J., Ao, C. O., and Li, K.: Estimating climatological planetary boundary layer heights from radiosonde observations: Comparison of methods and uncertainty analysis, Journal of Geophysical Research-Atmospheres, 115, 10.1029/2009jd013680, 2010.

Shen, J., Zhang, Y., Wang, X., Li, J., Chen, H., Liu, R., Zhong, L., Jiang, M., Yue, D., Chen, D., and Lv, W.: An ozone episode over the Pearl River Delta in October 2008, Atmospheric Environment, 122, 852-863, 10.1016/j.atmosenv.2015.03.036, 2015.

Shu, L., Xie, M., Wang, T., Gao, D., Chen, P., Han, Y., Li, S., Zhuang, B., and Li, M.: Integrated studies of a regional ozone pollution synthetically affected by subtropical high and typhoon system in the Yangtze River Delta region, China, Atmospheric Chemistry and Physics, 16, 15801-15819, 10.5194/acp-16-15801-2016, 2016.

Sillman, S.: The relation between ozone, NO_x and hydrocarbons in urban and polluted rural environments, Atmospheric Environment, 33, 1821-1845, 10.1016/s1352-2310(98)00345-8, 1999.

Solomon, P., Cowling, E., Hidy, G., and Furiness, C.: Comparison of scientific findings from major ozone field studies in North America and Europe, Atmospheric Environment, 34, 1885-1920, 10.1016/s1352-2310(99)00453-7, 2000.

Tang, G., Zhu, X., Xin, J., Hu, B., Song, T., Sun, Y., Zhang, J., Wang, L., Cheng, M., Chao, N., Kong, L., Li, X., and Wang, Y.: Modelling study of boundary-layer ozone over northern China - Part I: Ozone budget in summer, Atmospheric Research, 187, 128-137, 10.1016/j.atmosres.2016.10.017, 2017.

Wang, T., Ding, A., Gao, J., and Wu, W. S.: Strong ozone production in urban plumes from Beijing, China, Geophysical Research Letters, 33, 10.1029/2006gl027689, 2006a.

Wang, T., Xue, L., Brimblecombe, P., Lam, Y. F., Li, L., and Zhang, L.: Ozone pollution in China: A review of concentrations, meteorological influences, chemical precursors, and effects, Sci Total Environ, 575, 1582-1596, 10.1016/j.scitotenv.2016.10.081, 2017.

Wang, T. J., Lam, K. S., Xie, M., Wang, X. M., Carmichael, G., and Li, Y. S.: Integrated studies of a photochemical smog episode in Hong Kong and regional transport in the Pearl River Delta of China, Tellus Series B-Chemical and Physical Meteorology, 58, 31-40, 10.1111/j.1600-0889.2005.00172.x, 2006b.

Wang, Z., Li, J., Wang, X., Pochanart, P., and Akimoto, H.: Modeling of regional high ozone episode observed at two mountain sites (Mt. Tai and Huang) in East China, Journal of Atmospheric Chemistry, 55, 253-272, 10.1007/s10874-006-9038-6, 2006c.

Whaley, C. H., Strong, K., Jones, D. B. A., Walker, T. W., Jiang, Z., Henze, D. K., Cooke, M. A., McLinden, C. A., Mittermeier, R. L., Pommier, M., and Fogal, P. F.: Toronto area ozone: Long-term measurements and modeled sources of poor air quality events, Journal of Geophysical Research-Atmospheres, 120, 11368-11390, 10.1002/2014jd022984, 2015.

Yang, Y., Liao, H., and Li, J.: Impacts of the East Asian summer monsoon on interannual variations of summertime surface-layer ozone concentrations over China, Atmospheric Chemistry and Physics, 14, 6867-6879, 10.5194/acp-14-6867-2014, 2014.

Zhang, H., Wang, Y., Hu, J., Ying, Q., and Hu, X.-M.: Relationships between meteorological parameters and criteria air pollutants in three megacities in China, Environmental Research, 140, 242-254, 10.1016/j.envres.2015.04.004, 2015.

Zhang, H., Wang, Y., Park, T.-W., and Deng, Y.: Quantifying the relationship between extreme air pollution events and extreme weather events, Atmospheric Research, 188, 64-79, 10.1016/j.atmosres.2016.11.010, 2017.

Zhang, Y., Seidel, D. J., and Zhang, S.: Trends in Planetary Boundary Layer Height over Europe, Journal of Climate, 26, 10071-10076, 10.1175/jcli-d-13-00108.1, 2013.

Zhang, Y., and Wang, Y.: Climate-driven ground-level ozone extreme in the fall over the Southeast United States, Proc Natl Acad Sci U S A, 113, 10025-10030, 10.1073/pnas.1602563113, 2016.

Zhao, Z. J., and Wang, Y. X.: Influence of the West Pacific subtropical high on surface ozone daily variability in summertime over eastern China, Atmospheric Environment, 170, 197-204, 10.1016/j.atmosenv.2017.09.024, 2017.

Zheng, B., Tong, D., Li, M., Liu, F., Hong, C., Geng, G., Li, H., Li, X., Peng, L., Qi, J., Yan, L., Zhang, Y., Zhao, H., Zheng, Y., He, K., and Zhang, Q.: Trends in China's anthropogenic emissions since 2010 as the consequence of clean air actions, Atmospheric Chemistry and Physics, 18, 14095-14111, 10.5194/acp-18-14095-2018, 2018.

Zhou, D., Ding, A., Mao, H., Fu, C., Wang, T., Chan, L. Y., Ding, K., Zhang, Y., Liu, J., Lu, A., and Hao, N.: Impacts of the East Asian monsoon on lower tropospheric ozone over coastal South China, Environmental Research Letters, 8, 044011, 10.1088/1748-9326/8/4/044011, 2013.

Tables

Table 1: Net changes (NC) in O_3 mass~~Mass flux (MF~~ (Gg O_3 day^{-1})~~)~~ and percentage contributions (PC (%)) of different processes to O_3 in North China (36.5°N-40.5°N, 114.5°E-119.5°E) from surface to 850 hPa.

	Average [a]		OPEs [b]		OPEs-Average [c]
	NC (Gg O_3 day^{-1})	PC (%)	NC (Gg O_3 day^{-1})	PC (%)	NC (Gg O_3 day^{-1})
Net Chemical production	9.6	41.2	12.7	46.3	+3.3
Diffusion	0.4	1.6	-0.7	-2.6	-1.1
Dry deposition	-4.9	-20.9	-5.3	-19.3	-0.4
Horizontal advection	1.7	7.2	-7.4	-27.0	-9.1
Vertical advection	-6.8	-29.1	1.3	4.7	+8.1

[a]Average indicates the mean ~~MF~~ NC in O_3 mass and PC averaged over May to July of 2014-2017. [b]OPEs indicate the averaged ~~MF~~ NC in O_3 mass and PC for the ~~14~~ 15 OPEs that are captured by the GEOS-Chem model with I_OPE>0. [c]OPEs-Average indicate the differences in ~~MF~~ NC in O_3 mass between OPEs and Average.

Figures

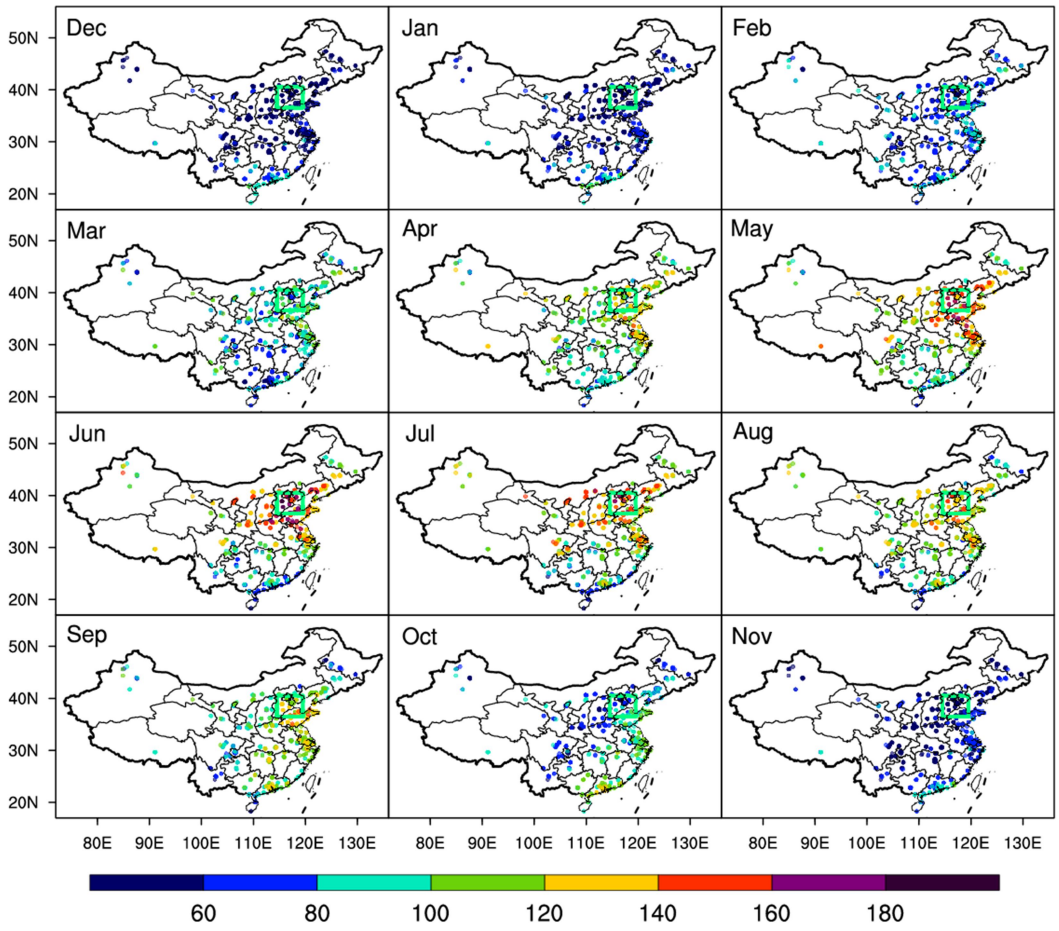

Figure 1: Monthly MDA8 O_3 concentrations (μg m^{-3}) averaged over 2014-2017 at 740 observational sites. The green solid lines enclose the North China region.

5

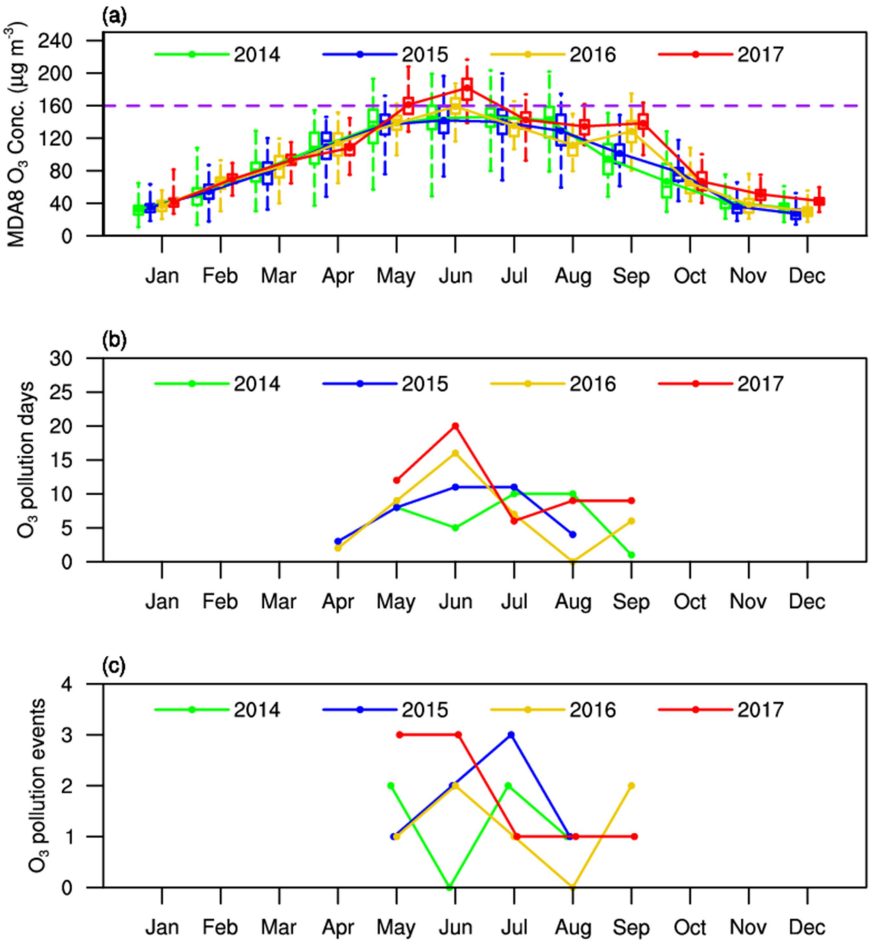

Figure 2: (a) Monthly variation in MDA8 O_3 concentration (μg m^{-3}) averaged over North China for 2014 to 2017. The boxes indicate the maximum and minimum MDA8 O_3 concentrations for 62 observational sites in North China. Dotted solid lines denote the averaged values in North China. The purple dashed line indicates the threshold of 160 μg m^{-3} for O_3 polluted days. (b) Monthly variation of O_3 polluted days in North China for 2014-2017. (c) Monthly variation of the number of ozone polluted events (OPEs) in North China for 2014-2017.

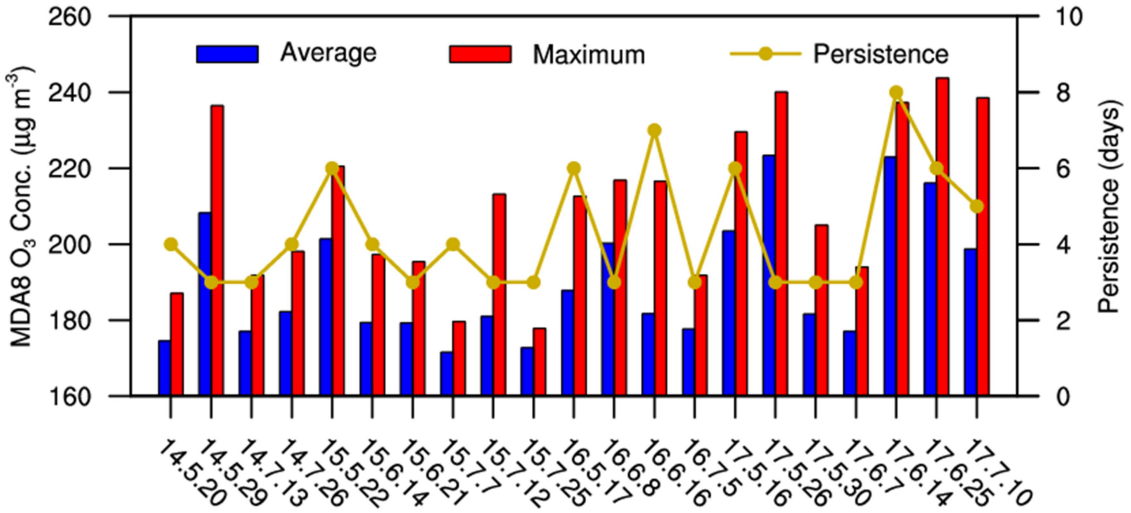

Figure 3: Mean (blue bars) and maximum (red bars) MDA8 O_3 concentrations (µg m^{-3}) averaged over North China for each of the 21 OPEs that occurred during May-July of 2014-2017. The dotted yellow line indicates the persistence (days) of each OPE.

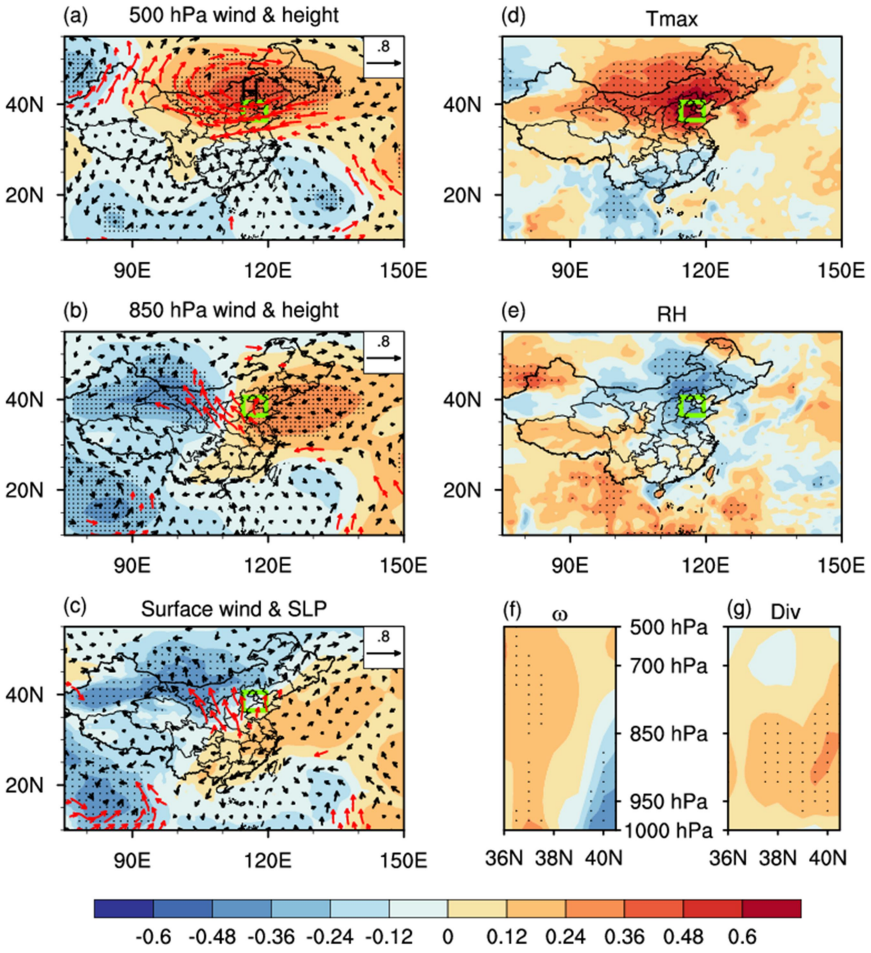

Figure 4: Composites of (a) wind field and geopotential height at 500 hPa, (b) wind field and geopotential height at 850 hPa, (c) surface wind field and SLP, (d) Tmax at the surface, (e) RH at the surface, (f) pressure-latitude cross-section of vertical pressure velocity (ω, positive value indicates downward air flow), and (g) pressure-latitude cross-section of divergence (positive value indicates divergence) for the 21 OPEs in North China. The data shown are composited over the ~~detrended and~~ standardized time series during May-July of 2014-2017 (see Sect. ~~4.1~~2.2). The green solid lines enclose North China. The red vectors in (a)-(c) and black dots in (a)-(g) are significant winds and parameters at 95% confidence.~~The red vectors in (a)-(c) highlight the important circulation features for OPEs.~~ The cross-sections are averaged over the longitudes of 114.5°E-119.5°E.

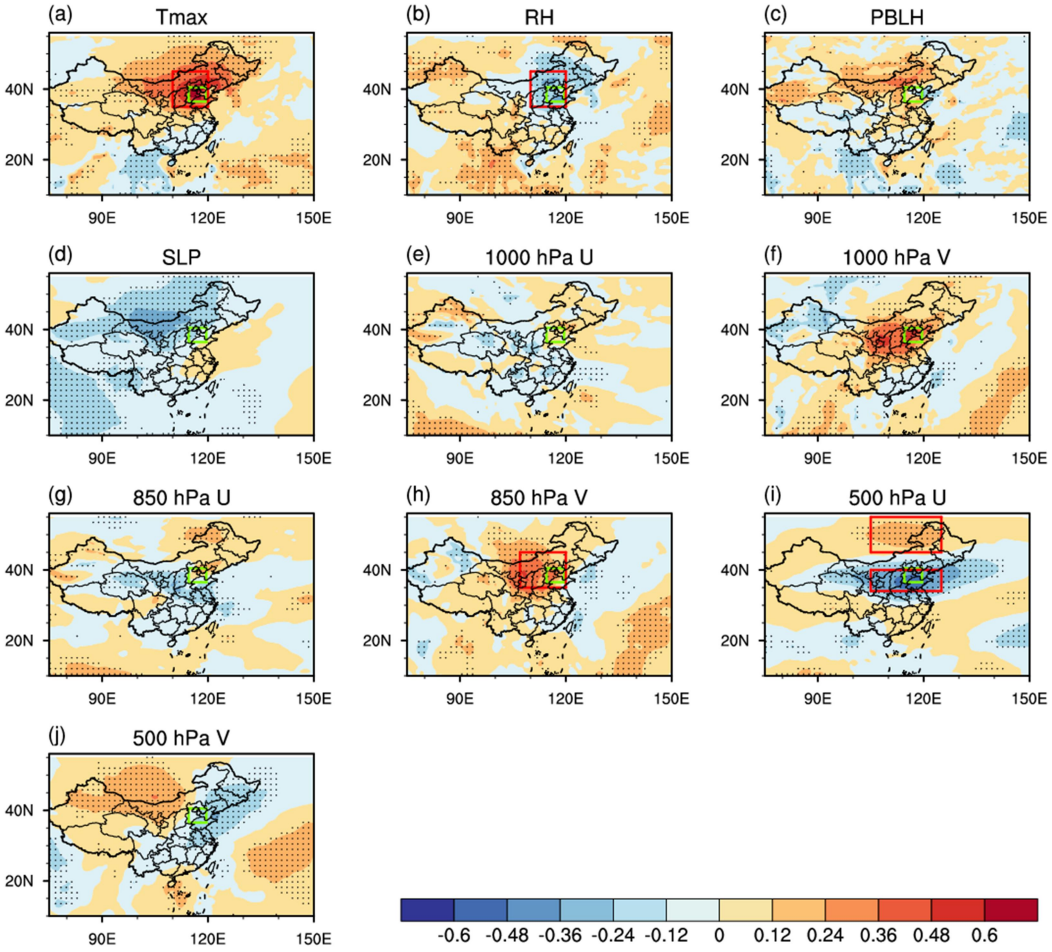

Figure 5: Correlation coefficients, for May to July of 2014-2017, between daily regional mean MDA8 O_3 concentrations in North China and daily mean (a) 2-meter Tmax at the surface, (b) RH at the surface, (c) planetary boundary layer height, (d) surface level pressure, (e) meridional winds at 1000 hPa, (f) zonal winds at 1000 hPa, (g) meridional winds at 850 hPa, (h) zonal winds at 850 hPa, (i) meridional winds at 500 hPa, and (j) zonal winds at 500 hPa in Asia. Correlation coefficients with black dots are statistically significant above the 95% confidence level. ~~Colored regions are correlation coefficients that are statistically significant above the 99 % confidence level.~~ The red rectangles in (a), (b), (h) and (i) denote the regions for calculating index_Tmax, index_RH, index_V850 and index_U500, respectively (see Sect. 4.3). The green rectangle indicates the region of North China.

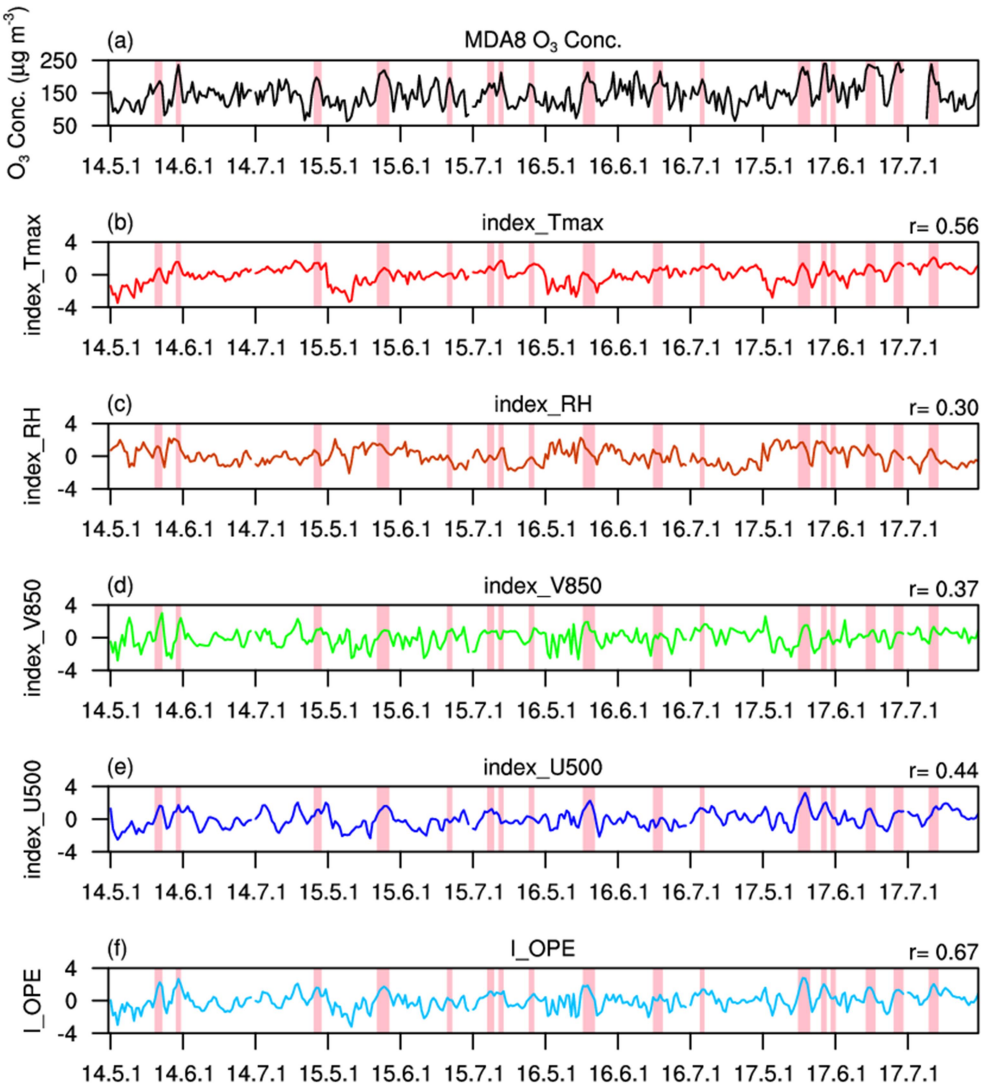

Figure 6: Daily variations in (a) MDA8 O_3 concentrations (μg m^{-3}) in North China, (b) index_Tmax, (c) index_RH, (d) index_V850, (e) index_U500, and (f) I_OPE for May-July of 2014-2017. Observed OPEs in North China are highlighted by pink rectangles. Correlation coefficients between MDA8 O_3 concentrations and different indexes are shown above the top right corner of each plot.

~~**Figure 7: Weather conditions for OPEs in North China. Left column shows composites of weather conditions for observed OPEs (on the basis of observed O_3 concentrations) for (a) anomalous Tmax, (b) anomalous RH, (c) anomalous wind vectors at 850 hPa (shades indicate meridional flow) and (d) anomalous wind vectors at 500 hPa (shades indicate zonal flow). (e)-(h), the same as (a)-(d), respectively, but show composites of weather conditions for days with I_OPE>0. The data shown are composited over the detrended and standardized time series during May-July of 2014-2017 (see Sect. 4.1). The green solid lines enclose North China**~~

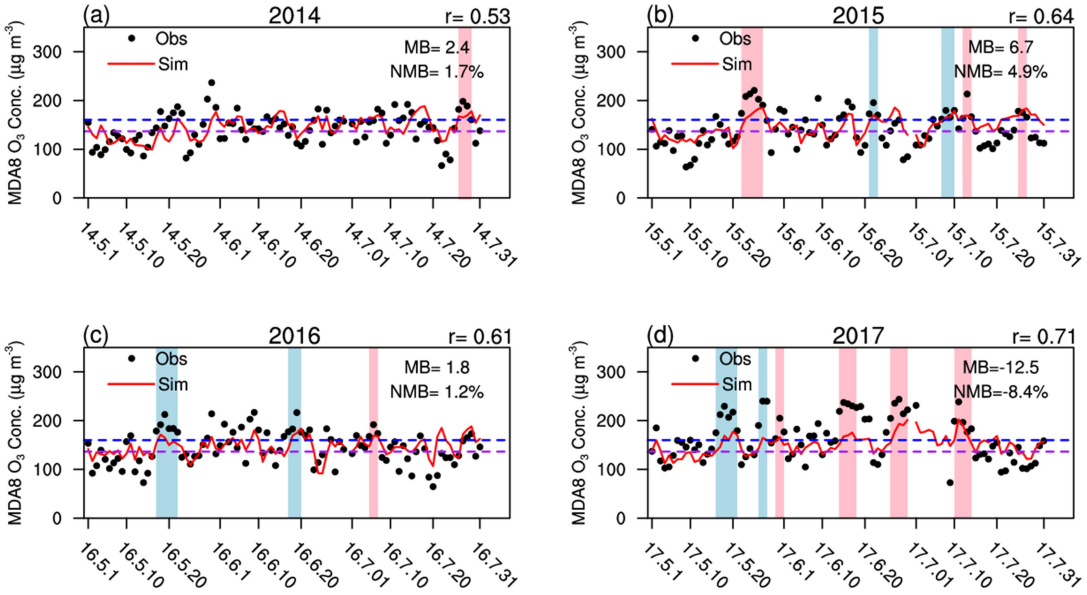

Figure 87: Daily variations in observed (black dots) and simulated (red solid lines) regional mean MDA8 O_3 (μg m^{-3}) in North China during May to July of 2014-2017. The blue and purple dashed lines indicate the thresholds of 160 μg m^{-3} and 136.6 μg m^{-3} for observation and simulation, respectively. OPEs captured by the GEOS-Chem model with I_OPE>0 are highlighted by pink rectangles (OPEs with simulated MDA8 O_3 concentrations larger than 160 μg m^{-3}) and by blue rectangles (OPEs with simulated MDA8 O_3 concentrations larger than 136.6 μg m^{-3} but including days with simulated MDA8 O_3 smaller or equal to 160 μg m^{-3}). Correlation coefficient between observed and simulated MDA8 O_3 concentrations for each year is shown above the top right corner of each plot. The mean bias (MB) and normalized mean bias (NMB) are calculated by $MB = \frac{1}{n}\sum_i^n (S_i - O_i)$ and $NMB = \sum_i^n (S_i - O_i) / \sum_i^n O_i * 100\,\%$, where O_i and S_i indicate the observed and simulated MDA8 O_3 concentrations on the i day, respectively, and n indicates the number of days.

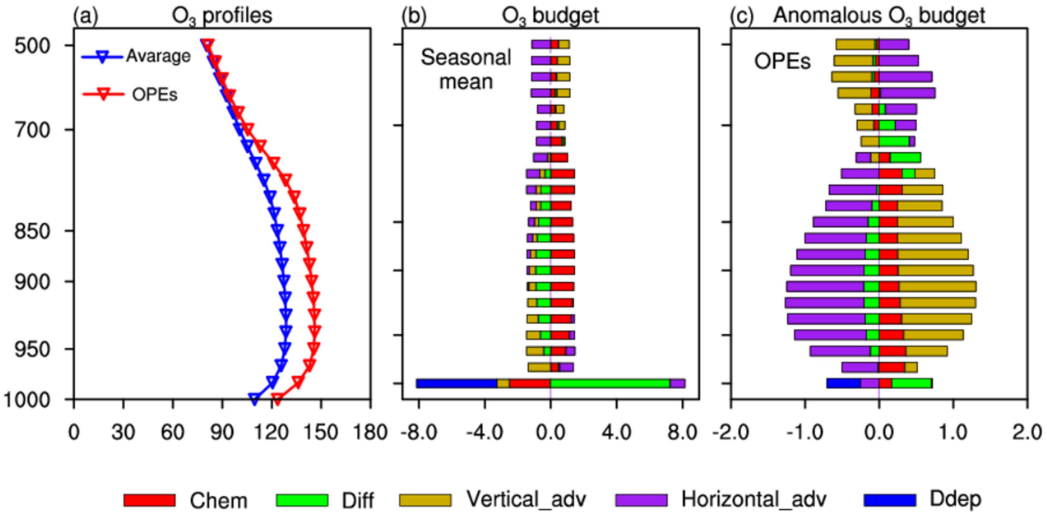

Figure ~~98~~: (a) Vertical profile of simulated daily O_3 concentrations (μg m^{-3}) averaged over May to July in 2014-2017 (blue line and triangle) as well as that composited over the 15 simulated OPEs with I_OPE>0 (red line and triangle) in North China. (b) Vertical profile of net change in O_3 mass (Gg O_3 day^{-1}) over North China for each process that is averaged over all days in May-July of 2014-2017. (c) Anomalous vertical profile of each process during the 15 OPEs relative to the mean value of May-July of 2014-2017. The vertical axis is the same for all the panels with a unit of hPa.~~(a) Vertical profile of O_3 mass flux (Gg O_3 day^{-1}) over North China for each process that is averaged over all days in May-July of 2014-2017. (b) Anomalous vertical profile of each process during the 14 OPEs relative to the mean value of May-July of 2014-2017. The 14 OPEs are captured by the GEOS-Chem model with I_OPE>0 in North China.~~

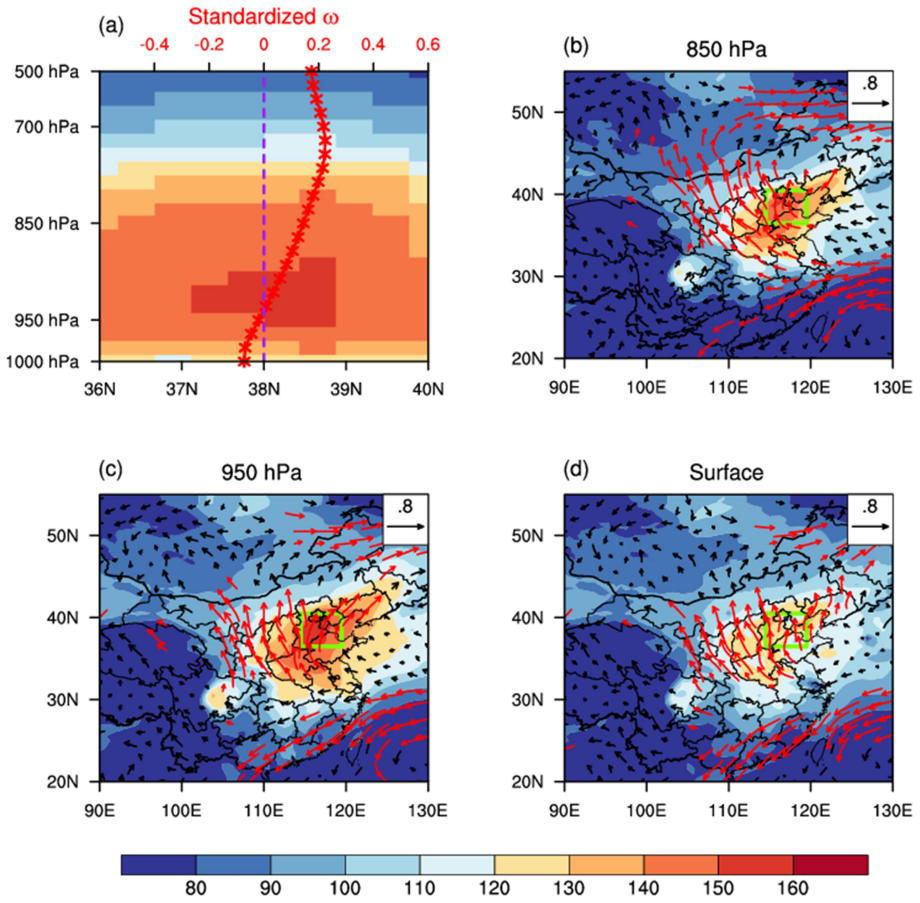

Figure ~~10~~9: (a) The pressure-latitude cross-section averaged over the longitudes of 114.5°E-119.5°E of simulated daily mean O_3 concentrations (μg m^{-3}) during the ~~14~~ 15 OPEs that are captured by the GEOS-Chem model with I_OPE>0. The red line with asterisks shows the anomalous profile of the regionally averaged vertical pressure velocity (ω, Pa s^{-1}, positive value indicates downward airflow) in North China. The purple dashed line indicates the position where the standardized ω is zero. (b)-(d) show anomalous winds and the simulated daily mean O_3 concentrations during OPEs at (b) 850 hPa, (c) 950 hPa and (d) the surface. The green solid lines enclose North China. ω in (a) and winds in (b)-(d) are composited over the ~~detrended and~~ standardized time series during May-July of 2014-2017 (see Sect. ~~4.1~~2.2). The red vectors in (b)-(d) are significant winds at 95% confidence.

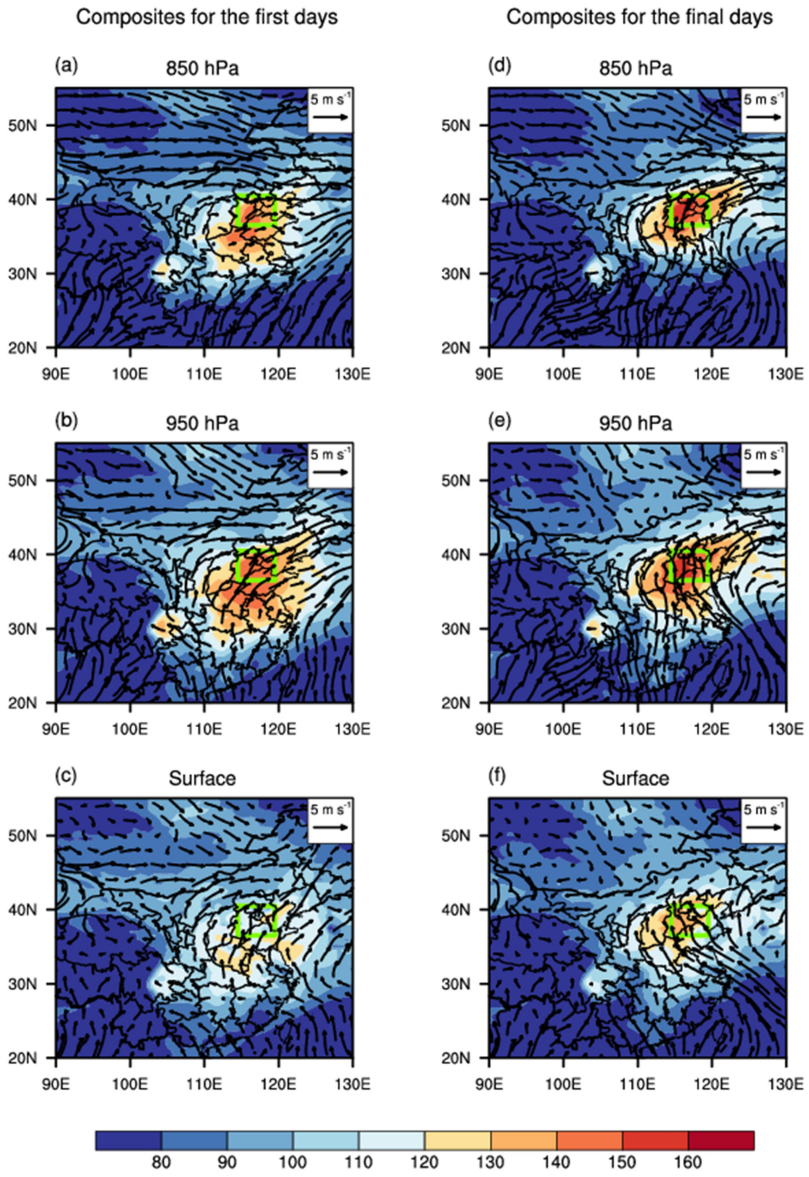

Figure ~~11~~10: Winds (m s^{-1}) and the simulated O_3 concentrations (μg m^{-3}) averaged over the first day of the ~~14~~ 15 OPEs that are captured by the GEOS-Chem model with I_OPE>0 at (a) 850 hPa, (b) 950 hPa and (c) the surface. (d)-(f) are the same as (a)-(c) but are averaged over the final day of the OPEs. The green solid lines enclose North China.

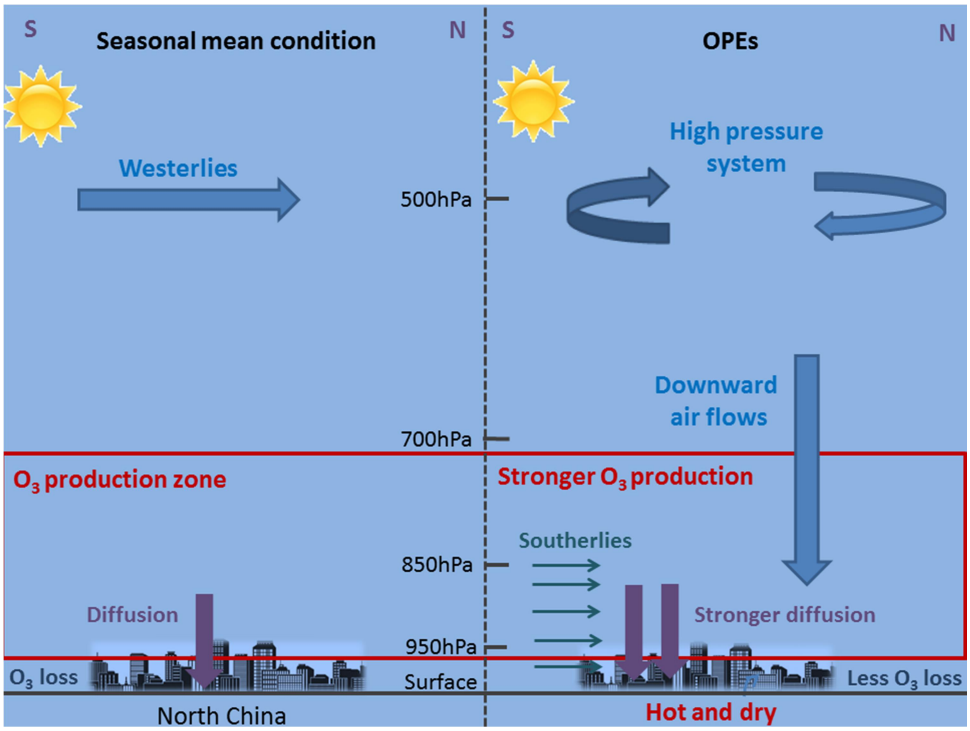

Figure 11. A schematic diagram of the typical weather pattern showing the mechanisms for the formation of OPEs in North China

Response to Comments of Reviewer #1

Manuscript number: acp-2019-263

Authors: Cheng Gong and Hong Liao

Title: A typical weather pattern for the ozone pollution events in North China

General comments:

This study examined the possible mechanisms for the ozone pollution events (OPEs) in North China during 2014-2017 using GEOS-Chem model together with an integrated process rate (IPR) analysis. They found that OPEs in North China occurred under a typical weather pattern with high daily maximum temperature, low relative humidity, anomalous southerlies and an anomalous downward air flow caused by an anomalous high-pressure system at 500 hPa. The topic is of interest, the method is sound. I would suggest for publication after addressing my comments below.

Response:

Thanks to the reviewer for the helpful comments and suggestions. We have revised the manuscript carefully and the point-to-point responses are listed below.

Specific Comments:

Page 2 Lines 11 -13: Please reframe this sentence

Response:

We have reframed this sentence as:

'Zhang et al. (2015) showed that values of RH for days with top 10% O_3 concentrations were lower compared to those for days with bottom 10% O_3 concentrations by examining continuous observations of O_3 and meteorological parameters in Guangzhou during March 2013 to February 2014.'

Page 4 Lines 14-15: I don't think the original resolution of MERRA2 data is the same as GEOS-Chem model. The meteorological data authors used are modified to fit the model resolution.

Response:

We have revised the sentence to clarify: 'The original MERRA2 data has a horizontal resolution of 0.5° latitude x 0.625° longitude and 72 vertical layers (Molod et al., 2015). The GEOS-Chem model has the same horizontal resolution over the nested domain but the GEOS-Chem support team has lumped the 72 vertical layers into 47 layers to save computational resources. The lumped vertical levels are within the 32th model layer (about 190 hPa) and the top of atmosphere (about 0.01 hPa).'

Page 4 Lines 23-24: How did the authors detrend the meteorological parameters to

remove interannual or seasonal variability? Please specify the method or provide formula they used.

Response:

Following the reviewer's comments, we have compared our analyses with and without detrending and found small impact on our results because of the relatively short time period (only 4 years over 2014-2017). To avoid confusion, we have removed the detrending process and updated the table and figures in the revised manuscript. The description here has been revised as follows:

'The daily time series of a meteorological parameter x at a specific model grid cell over May to July of 2014-2017 is standardized by:

$$[x_i] = \frac{x_i - \frac{\sum_i^n x_i}{n}}{s_i} \quad (1)$$

where x_i indicates the parameter x on day i, n is the total number of days over May to July in 2014-2017, s_i indicates the standard deviation of the daily time series. $[x_i]$ is the standardized anomaly for parameter x on day i.'

Page 5 Line 7: The annual emission from 2014 to 2017 are applied in the simulation, but the authors did not rule out the impacts of changing emissions on the OPEs selection and IPR analysis, although the changes in emissions in the four years are not likely to be very large.

Response:

We use emissions from 2014 to 2017 in the model to obtain OPEs with realistic changes in emissions. Following your suggestion, we have carried out a new simulation by fixing anthropogenic emissions at year 2014 levels. Twelve of the 17 observed OPEs with I_OPE >0 can be identified by applying the same threshold (136.6 μg m^{-3}) in the model (Figure R1). Compared with the simulation with year-by-year changes in emissions from 2014 to 2017, three OPEs (one in June of 2015, one in July of 2016, and one in May of 2017) are missed in the run with fixed emissions. The results from IPR analysis with fixed emissions are similar to those with changes in emissions except that the simulation with fixed emissions has lower changes in O_3 mass by net chemical production due to the changes in NO_x/VOCs ratio (Li et al., 2019). As a result, the changes in emissions have little impacts on the OPEs selection and IPR analysis (Figures R1 and R2 and Table R1).

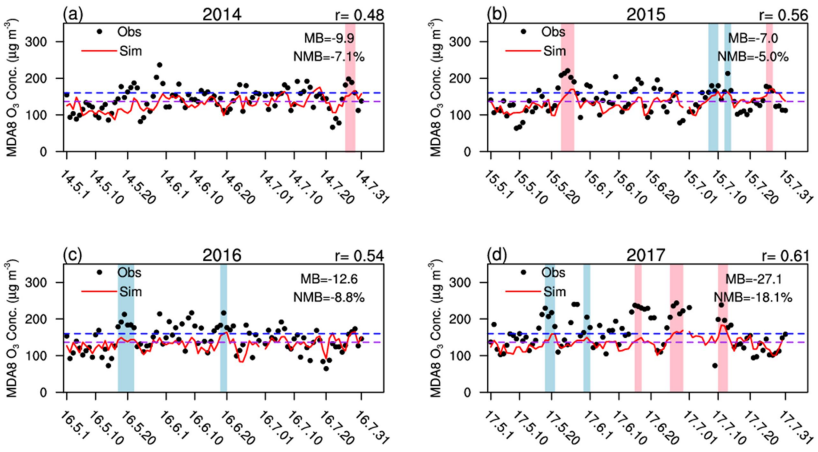

Figure R1. The same as Figure 7 in the revised manuscript but with fixed emissions at 2014 levels.

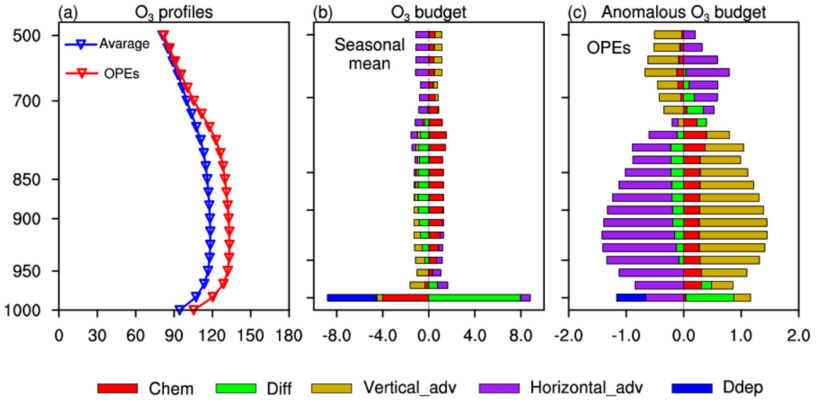

Figure R2. The same as Figure 8 in the revised manuscript but with fixed emissions at 2014 levels

Table R1. The same as Table 1 in the revised manuscript but with fixed emissions at 2014 levels.

	Average [a]		OPEs [b]		OPEs-Average [c]
	NC ($Gg\ O_3\ day^{-1}$)	PC (%)	NC ($Gg\ O_3\ day^{-1}$)	PC (%)	MF ($Gg\ O_3\ day^{-1}$)
Net Chemical production	4.6	21.8	7.5	28.8	+2.9
Diffusion	2.4	11.4	2.1	8.1	-0.3
Dry deposition	-4.3	-20.4	-4.8	-18.5	-0.5
Horizontal advection	3.5	16.6	-8.0	-30.8	-11.5
Vertical advection	-6.3	-29.8	3.6	13.8	+9.9

Figures: All the figures and analysis are lack of significance test. Please add in.

Response:

We have added the significance test with 95 % confidence in Figures 4, 5, 9 and S2 in the revised manuscript and supplementary material.

Page 7 Line 9: I on day 'd'.

Response:

The 'd' has been added.

Page 8 Line 9: It should be 850 hPa 'meridional winds' and 500 hPa 'zonal' winds.

Response:

Corrected.

Page 11 Line 9: Before analyzing vertical profiles of each process, the authors should give vertical profile of O3 concentrations in terms of seasonal mean and anomalies during OPEs.

Response:

Following the reviewer's suggestion, we have added a new panel in Fig. 8 (Fig. 8a) in the revised manuscript to show the vertical profiles of O_3 concentrations in terms of seasonal mean and anomalies during OPEs. We have also added the following sentences to describe these vertical profiles of O_3 in the text:

'The vertical profile of simulated daily O_3 concentrations averaged over May to July in 2014-2017 as well as that composited over the 15 OPEs are shown in Fig. 8a. For both profiles, the O_3 concentrations are highest between 950 hPa and 850 hPa and are relatively lower at the surface due to the titration by high NO_x concentrations. When OPEs occur, O_3 concentrations are higher from the surface to 700 hPa (about 3 km altitude) but change little above 700 hPa, indicating that the enhancement of O_3 concentrations during OPEs occurs not only at the surface but also in and above the boundary layer.'

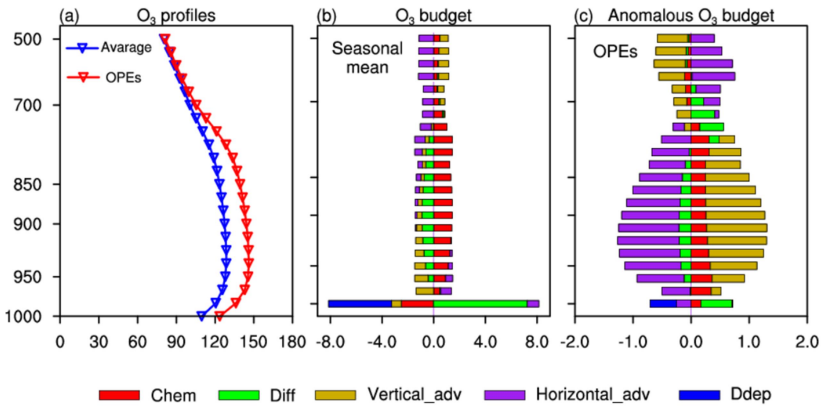

Figure 8. (a) Vertical profile of simulated daily O_3 concentrations (μg m^{-3}) averaged over May to July in 2014-2017 (blue line and triangle) as well as that composited over the 15 simulated OPEs with I_OPE>0 (red line and triangle) in North China. (b) Vertical profile of O_3 mass flux (Gg O_3 day^{-1}) over North China for each process that is averaged over all days in May-July of 2014-2017. (c) Anomalous vertical profile of each process during the 15 OPEs relative to the mean value of May-July of 2014-2017. The vertical axis is the same for all the panels with a unit of hPa.

Page 11 Line 24: 'horizontal advection' is the compensating from the increasing ozone from the figure. I don't think it should be listed as the dominant processes that lead to OPEs, although the negative value is large.

Response:

'horizontal advection' has been removed.

References:

Li, K., Jacob, D. J., Liao, H., Shen, L., Zhang, Q., and Bates, K. H.: Anthropogenic drivers of 2013-2017 trends in summer surface ozone in China, Proceedings of the National Academy of Sciences of the United States of America, 116, 422-427, 10.1073/pnas.1812168116, 2019.

Molod, A., Takacs, L., Suarez, M., and Bacmeister, J.: Development of the GEOS-5 atmospheric general circulation model: evolution from MERRA to MERRA2, Geoscientific Model Development, 8, 1339-1356, 10.5194/gmd-8-1339-2015, 2015.

Response to Comments of Reviewer #2

Manuscript number: acp-2019-263

Authors: Cheng Gong and Hong Liao

Title: A typical weather pattern for the ozone pollution events in North China

General comments:

General comments: Ozone pollution in China is becoming a noticeable problem particularly in summer season. This paper focuses on this problem in north China region. Two parts of work have done. One is a long term (4 years) analysis of the ozone pollution status. Ozone pollution days and events are defined and identified in the research years. Using these days/events, the so called correspondent weather pattern are composited. The second part of work is to establish an index to identify the ozone pollution day/event. Using GEOS-Chem model, simulation results for these 4 summers are used to support the index.

The ozone pollution status is clearly shown. The related weather pattern seems a reasonable but anticipative result. The GEOS-Chem simulation provides results not so informative

Response:

Understanding the weather pattern that leads to OPEs is important for better understanding the formation of OPEs and for forecasting OPEs on daily scale. Previous studies that examined OPEs and the associated weather patterns in China were generally focused on one or two episodes of high O_3 concentrations at specific locations, such as Mountains Tai and Huang (Wang et al., 2006), Hangzhou (Li et al., 2017a), Shanghai and Nanjing (Shu et al., 2016). Our work reports a typical 3-D weather pattern for OPEs in North China on the basis of national air quality monitoring data and reanalyzed meteorological fields for 2014-2017, which is a more representative and systematic investigation compared with previous studies.

The typical weather pattern is characterized by high temperature and low humidity at the surface, anomalous southerlies and divergence in the lower troposphere (from surface to 850 hPa), high pressure system at 500 hPa and downward air flows from 500 hPa to the surface. Although high temperature and low humidity have been reported in previous studies (e.g. Zhang and Wang, 2016; Pu et al., 2017; Zhang et al., 2017), we find some new features for the formation of OPEs in North China (such as the downward airflow and southerlies).

We carry out process analysis using the GEOS-Chem model to identify the dominant processes that lead to OPEs, which, to our knowledge, is the first study to have such quantitative examination of the weather pattern to understand the mechanisms for the formation of OPEs. Our analyses show that the net chemical production is the most dominate process for the seasonal mean condition, however, when OPEs occur, the most dominant process is vertical advection that leads to the largest net increase in O_3

mass from the surface to 850 hPa. We have added a schematic diagram of the typical weather pattern showing the mechanisms for the formation of OPEs in North China (a new Fig. 11 in the revised manuscript).

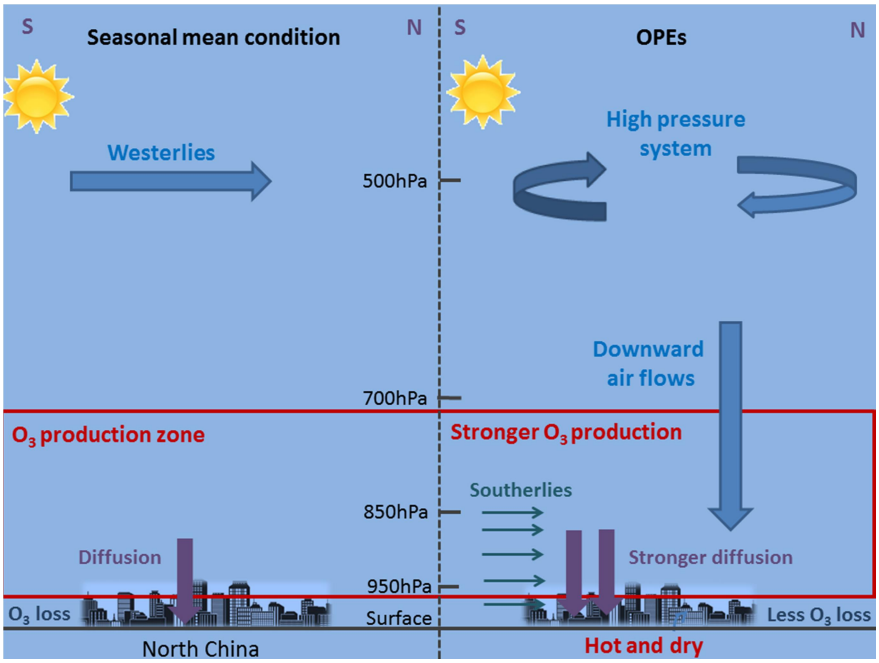

Figure 11. A schematic diagram of the typical weather pattern showing the mechanisms for the formation of OPEs in North China

Specific Comments:

1. *It is well known that the ozone pollution is related to sunny days, high temperature, precursors, boundary layer process, etc. Once the high ozone events are selected, the statistics of weather pattern is just a conditional sampling result, so that the features are anticipative.*

Response:

See our responses to your general comments.

2. *The selection of Index_U500 seems quite arbitrary. What does it mean by the wind speed difference of two zones? What is the reason to choose these two zones? Is it ok the zones larger or smaller?*

Response:

The main purpose of using index_U500 is to represent the high-pressure system at 500 hPa level during OPEs relative to the seasonal mean conditions (Fig. 4a). Since the high-pressure system is characterized by anti-cyclone circulation, the index_U500 is defined as the difference in zonal winds (westerlies are positive) between the northern region (supposed to be westerlies) and the southern region (supposed to be easterlies) of the typical high-pressure system (Eq. (7)). As a result, the index_U500 can be used to describe whether the high-pressure system exists (index_U500 >0) or not (index_U500<0). Higher index_U500 indicates stronger anti-cyclone circulation

and stronger high-pressure system. A similar method has been used in the previous study of Cai et al. (2017).

The regions for the calculation of index_x (including index_U500) in Eq.3 are selected on the basis of the correlations between MDA8 O_3 concentrations in North China and the corresponding meteorological parameters (Fig. 5). Figure 5i shows that, for correlations between MDA8 O_3 concentrations and the zonal winds at 500 hPa, the correlation coefficients are the largest in the two regions enclosed by red rectangles; therefore these two regions are used for the definition of index_U500.

3. *GEOS-Chem simulation of ozone concentration does not agree to the observation satisfactorily in Figure 8.*

Response:

The GEOS-Chem model has been used to simulate O_3 in China and been evaluated extensively in previous studies (Wang et al., 2011; Yang et al., 2014; Lou et al., 2014; Lou et al., 2015; Ni et al., 2018; Li et al., 2019; Lu et al., 2019; Sun et al., 2019), which shows the GEOS-Chem model can capture fairly well the daily, monthly, seasonal, and interannual variations of O_3 in China. In our work, we evaluate mean bias (MB) and normalized mean bias (NMB) of simulated MDA8 O_3 concentrations averaged over North China by comparing with measurements. For the daily time series of MDA8 O_3 concentrations over May to July in 2014-2017, simulated concentrations have a mean MB (NMB) of 2.4 μg m^{-3} (1.7%) in 2014, 6.7 μg m^{-3} (4.9%) in 2015, 1.8 μg m^{-3} (1.2%) in 2016, and -12.5 μg m^{-3} (-8.4%) in 2017 (Figure 7), indicating that the GEOS-Chem model has a good performance. We do find that the GEOS-Chem model has difficulties in capturing the peak values of O_3 concentrations, which is a common issue in the GEOS-Chem model (Zhang and Wang, 2016; Ni et al., 2018), WRF-Chem (Tie et al., 2009) and WRF-CMAQ (Shu et al., 2016). In our analysis, the threshold for OPEs in the model has been revised as 136.6 μg m^{-3} (160*85.4 %) by applying the NMB of -14.6 % for the days with observed MDA8 O_3 > 160 μg m^{-3}. This modification enables us to identify 15 of 21 observed OPEs with I_OPE>0.

4. *The role of diffusion or mixing on ozone mass flux is not clearly described. At first, the authors declare "Note that the MF of each process at a specific level indicates the net O3 mass change within this level rather than the flux across this level, especially for the vertical processes such as diffusion and vertical advection", but at later, they state "it is indicated that O3 aloft is transported downward to be mixed at the surface by the diffusion process", and " Vertical advection exhibits negative MF values from the surface to approximately 750 hPa". We need to clarify it is the "mass flux" or the "mass flux divergence", the former indicates mass across the level, the latter is the net mass change.*

Response:

Thanks for the comments. To avoid confusion and also to take into account your comment on too many acronym (Other point #0), we have replaced ‘mass flux’ or MF

in the text by 'net change in O_3 mass' when we describe IPR for each process in a specific model layer.

5. *I think the ozone production is mainly within the atmospheric boundary layer, not above it. So it is not true: "hot air is beneficial for developing the mixed layer, leading to more O3 mixed downward to the surface during OPEs"*

Response:

As shown in Figure 8, O_3 production is large not only within the boundary layer (from 850 hPa to the surface) but also between 850 and 800 hPa, especially during the OPEs. We highlight that the vertical concentration gradient caused by O_3 chemical production at and above the upper boundary layer and chemical loss at the surface leads to downward transport of O_3 by diffusion process. We have revised this sentence to clarify:

'Moreover, hot and sunny weather during OPEs increases the vertical concentration gradient (stronger chemical production at and above the upper boundary layer), leading to more O_3 transported downward to the surface as described in Sect. 5.2.2.'

Other points:

0. *too many acronym, someone not necessary, for example, mass flux: MF.*

Response:

We have replaced 'mass flux' or MF in the text by 'net change in O_3 mass' when we describe IPR for each process in a specific model layer.

1. *Page 1 line19: "chemical production of O3 was high between 800 and 900 hPa", what height?*

Response:

The GEOS-Chem model describes vertical layers by hPa (see *http://wiki.seas.harvard.edu/geos-chem/index.php/GEOS-Chem_vertical_grids*). We have clarified here 'chemical production of O_3 was high between 800 and 900 hPa (approximately 0.8-1.8 km altitudes)'.

2. *Page 3, line 22: "Section 3 presents the observed and spatiotemporal distributions of OPEs in North China during 2014 to 2017", sentence not very clear.*

Response:

This sentence has been revised as:

'Section 3 presents the observed frequency and intensity of OPEs in North China during 2014-2017.'

3. *page 3: (http://datacenter.mep.gov.cn/websjzx/queryIndex.vm), no linkage.*

Response:

Since the name of Ministry of Environmental Protection (MEP) was changed to Ministry of Ecology and Environment (MEE), the website address is now http://datacenter.mee.gov.cn/websjzx/queryIndex.vm.

4. *page 4, line 2:"(67 sites among the 114 sites in North China (36°-40.5°N, 114.5°-119.5°E)) are selected and used in this study." Need more details or figure to show the 67 sites.*

Response:

Sorry for the inconsistent border over North China here, which should be (36.5°-40.5°N, 114.5°-119.5°E). We have added a new figure (Fig. S1) in the supplementary material to show these 62 sites. The sentence in the text has been revised as: 'As a result, 740 among the 1582 sites in China (62 sites among the 101 sites in North China (36.5°-40.5°N, 114.5°-119.5°E), Fig. S1) are selected and used in this study.'

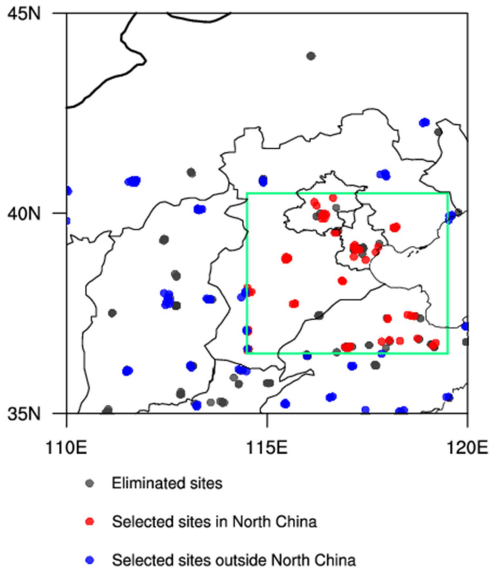

Figure S1. Distribution of the observational sites in North China. The gray dots indicate sites eliminated by the data quality control (see Sect. 2.1 for details). The red and blue dots indicate the selected sites inside and outside North China, respectively. The green rectangle encloses North China.

5. *Page 4, line 20: "MERRA2 dataset, daily mean geopotential heights at 850 hPa and 500 hPa from the National Center for Environmental Prediction (NCEP) . . .", MERRA2 and NCEP dataset, consistent? At least the resolution is different.*

Response:

The NCEP dataset is only used in Figure 4 for geopotential heights due to the lack of geopotential heights in MERRA2 dataset. In Figure 4, all of the meteorological parameters from MERRA2 and NCEP dataset have the same time period (May to July

over 2014-2017), time resolution (daily). The only difference between MERRA2 and NCEP datasets is the different spatial resolution (0.5° latitude x 0.625° longitude for MERRA2 and 2.5° latitude x 2.5° longitude for NCEP). However, it is not a problem in Figure 4 because the drawing software (NCAR Command Language, NCL) we utilized is able to contour the map automatically according to the resolution of the dataset.

6. *page 4, line 24:"All the time series of meteorological parameters have been detrended first and then standardized by their respective standard deviation to remove interannual or seasonal variability", what is the performance and result?*

Response:

Following the other reviewer's comments, we have compared our analyses with and without detrending and found small impact on our results, because of the relatively short time period (only 4 years over 2014-2017). To avoid confusion, we have removed the detrending process and updated the table and figures in the revised manuscript. The description here has been revised as follows:

'The daily time series of a meteorological parameter x at a specific model grid cell over May to July of 2014-2017 is standardized by:

$$[x_i] = \frac{x_i - \frac{\sum_i^n x_i}{n}}{s_i} \quad (1)$$

where x_i indicates the parameter x on day i, n is the total number of days over May to July in 2014-2017, s_i indicates the standard deviation of the daily time series. $[x_i]$ is the standardized anomaly for parameter x on day i.'

7. *page 6 line 1: "all 62 sites", previously 67 sites!*

Response:

The previous '67 sites' has been revised as '62 sites'.

8. *page 6, line 24: "last for many consecutive days. The mean duration of OPEs is 4.3 days, while some episodes can last for one week and even Longer". Can be interpreted by sub-tropical high, in summer.*

Response:

Climatically, the onset of sub-tropical high occurs in central and southern Indochina Peninsula in early May. Then sub-tropical high migrates northward in a stepwise fashion, characterized by two northward jumps in mid-June (to 20°-25°N) and in late July (to 25°-30°N or even north) (Ding and Chan, 2005; Su et al., 2014). As a result, the sub-tropical high can barely influence North China during our studied time period of May to July.

In synoptic meteorology, the regions with geopotential height larger than 5880 m at

500 hPa level are considered being controlled by sub-tropical high. By applying this definition and the NCEP dataset, the locations of sub-tropical high for each OPE in our analysis are represented (Figure R1). None of the OPEs in North China occurs under the sub-tropical high. Also, by comparing the geopotential height at 500 hPa averaged over May to July in 2014-2017 and the 21 OPEs, we find that the location of sub-tropical high change little (Figure R2, sub-tropical high is highlighted by the black dots). We believe that the high pressure system identified in our study is irrelevant with the sub-tropical high.

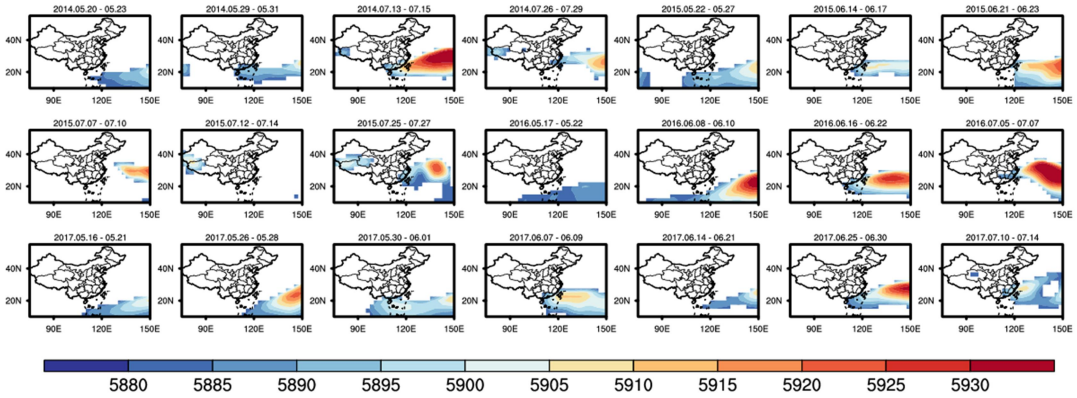

Figure R1. The mean geopotential height (m) at 500 hPa level for each OPE in North China. Only regions with geopotential height larger than 5880 m are colored to represent the locations of the sub-tropical high.

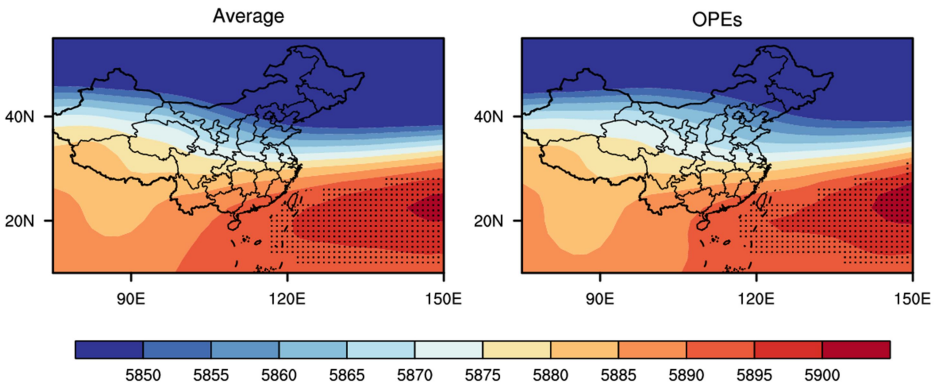

Figure R2. The geopotential height (m) at 500 hPa averaged over May to July in 2014-2017 (left) and over the 21 observed OPEs (right). The locations of sub-tropical high (geopotential height larger than 5880 m) are highlighted by the black dots.

9. *page 8 line 10: "850 hPa zonal winds indicate circulation in the lower atmosphere and 500 hPa meridional winds describe the dominate large-scale circulation", why take zonal winds at 850hPa?*

Response:

It has been revised as '850 hPa meridional winds indicate circulation in the lower atmosphere and 500 hPa zonal winds describe the dominate large-scale circulation'.

10. *Figure 5: why the calculation region for V_850hPa differently?*

Response:

As we explained in our response to your 'Specific Comment #2', the selection of calculating region for the index_V850 depends on the correlations shown in Fig. 5h. The strongest correlations between MDA8 O_3 concentrations and V850 occur in North China as well as the west region (enclosed by 35°N-45°N, 107°E - 120°E, the red rectangle in Fig. 5h).

11. *Figure 7, similar to Figure 4?*

Response:

Figure 4 shows the typical weather pattern for observed OPEs by composite analysis. Figure 7a-d is the same as Fig. 4d, 4e, 4b and 4a, respectively. However, Figure 7 is utilized to verify that the I_OPE, which is defined by meteorological fields only, can well represent the typical weather pattern obtained from observed OPEs. To address this concern, we have moved Figure 7 to be Figure S2 in the supplementary material.

12. *Page 9 line 21: "indicating that the GEOS-Chem model can simulate the daily variation in MDA8 O3", but the simulation not agree well to the observation in Figure 8.*

Response:

See our response to your 'Specific comments #3'.

13. *page 9 line 26: " The linear regression through the origin between observed and simulated MDA8 O3 has a regression coefficient of 0.96, indicating the capability of the model in simulating the MDA8 O3 concentrations." Need to be clarified.*

Response:

We have added Fig. S3 in the supplementary material to clarify the linear regression between observed and simulated MDA8 O_3 concentrations. The sentence has been revised as:

'The linear regression by the least square method through the origin between observed and simulated MDA8 O_3 has a regression coefficient of 0.96 (Fig. S3), indicating the capability of the model in simulating the MDA8 O_3 concentrations.'

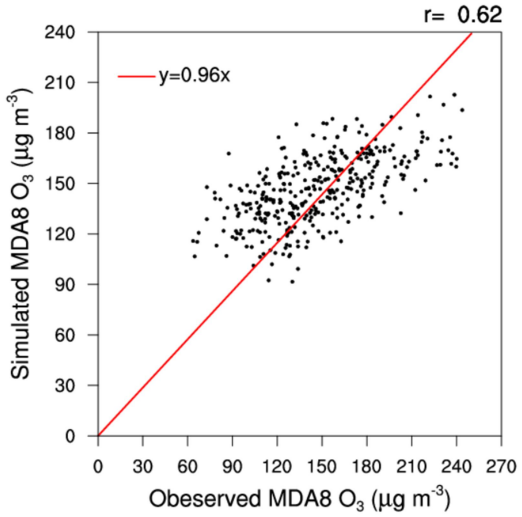

Figure S3. The linear regression through the origin between observed and simulated MDA8 O_3 concentrations (µg m^{-3}). The black dots indicate the daily observed and simulated MDA8 O_3 concentrations averaged over North China from May to July in 2014-2017, and the correlation coefficient between them are given at the top-right corner. The red line indicates the regression line through the origin calculated by the least square method.

14. *Page 10, line 29: "diffusion has a small effect on the total mass of O3 in the boundary layer. However, the diffusion process is important in 30 the boundary layer, which has . . .", confused.*

Response:

Sorry for the confusion. We have revised the second paragraph of Sect. 5.2.1 as:

'Diffusion process in GEOS-Chem model describes the mixing in the boundary layer, which transports O_3 along the concentration gradient. Since O_3 concentrations are higher at 950 hPa to 850 hPa than at the surface (Fig. 8a), the diffusion transports O_3 from the upper boundary layer downwardly to the surface. As a result, the IPR analysis shows that the net mass change in O_3 by diffusion is negative between 950 and 850 hPa but positive at the surface (Fig. 8b). Note that the net changes in O_3 mass over North China by diffusion process should approximately equal to zero (Table 1) if we integrate the change in O_3 mass by diffusion from the surface to 850 hPa because diffusion is an internal vertical transport. The downward transport of O_3 by diffusion was also reported in previous IPR analyses (e.g., Khiem et al., 2010; Li et al., 2012; Tang et al., 2017).

15. *'page 10 line 31: "mass flux of diffusion for the whole boundary layer is small, it is indicated that O_3 aloft is transported downward to be mixed at the surface by the diffusion process", very strange explanation.*

Response:

See our response above (our response to #14 of your Other points).

16. *Page 11 line 13: "both the positive contribution at the surface and the negative contributions in the upper layers increase", ok. "indicating that more O3 is mixed from the upper levels to the surface to increase the surface O3 concentration during OPEs", why mixing/diffusion increase surface O3?*

Response:

As we explained in our response to your 'Other points #14', for the seasonal mean condition, O_3 chemical production at and above the upper boundary layer leads to higher O_3 concentrations there than at the surface, causing the downward transport of O_3 by diffusion. During OPEs, hot and sunny conditions enhance O_3 chemical production at and above the upper boundary layer and hence more O_3 is transported from the upper boundary layer to the surface.

17. *Page 12 line 1: "beneficial for developing the mixed layer, leading to more O3 mixed downward to the surface during OPEs", O3 produces in the boundary layer, no need to mixing down from upper layer above ABL.*

Response:

See our response to your 'Specific comments #5'.

18. *page 13 line 14: "horizontal advection, and vertical advection are the most dominant processes that lead to OPEs", but horizontal advection contributes negative mass flux? So, not lead to OPEs, but depress the development of OPEs.*

Response:

The 'horizontal advection' has been removed in the revised manuscript.

References:

Cai, W., Li, K., Liao, H., Wang, H., and Wu, L.: Weather conditions conducive to Beijing severe haze more frequent under climate change, Nature Climate Change, 7, 257-+, 10.1038/nclimate3249, 2017.

Ding, Y. H., and Chan, J. C. L.: The East Asian summer monsoon: an overview, Meteorology and Atmospheric Physics, 89, 117-142, 10.1007/s00703-005-0125-z, 2005.

Khiem, M., Ooka, R., Hayami, H., Yoshikado, H., Huang, H., and Kawamoto, Y.: Process analysis of ozone formation under different weather conditions over the Kanto region of Japan using the MM5/CMAQ modelling system, Atmospheric Environment, 44, 4463-4473, 10.1016/j.atmosenv.2010.07.038, 2010.

Li, K., Chen, L., Ying, F., White, S. J., Jang, C., Wu, X., Gao, X., Hong, S., Shen, J., Azzi, M., and Cen, K.: Meteorological and chemical impacts on ozone formation: A case study in Hangzhou, China, Atmospheric Research, 196, 40-52, 10.1016/j.atmosres.2017.06.003, 2017a.

Li, K., Jacob, D. J., Liao, H., Shen, L., Zhang, Q., and Bates, K. H.: Anthropogenic drivers of 2013-2017 trends in summer surface ozone in China, Proceedings of the National Academy of Sciences of the United States of America, 116, 422-427, 10.1073/pnas.1812168116, 2019.

Li, L., Chen, C. H., Huang, C., Huang, H. Y., Zhang, G. F., Wang, Y. J., Wang, H. L., Lou, S. R., Qiao,

L. P., Zhou, M., Chen, M. H., Chen, Y. R., Streets, D. G., Fu, J. S., and Jang, C. J.: Process analysis of regional ozone formation over the Yangtze River Delta, China using the Community Multi-scale Air Quality modeling system, Atmospheric Chemistry and Physics, 12, 10971-10987, 10.5194/acp-12-10971-2012, 2012.

Lou, S., Liao, H., and Zhu, B.: Impacts of aerosols on surface-layer ozone concentrations in China through heterogeneous reactions and changes in photolysis rates, Atmospheric Environment, 85, 123-138, 10.1016/j.atmosenv.2013.12.004, 2014.

Lou, S., Liao, H., Yang, Y., and Mu, Q.: Simulation of the interannual variations of tropospheric ozone over China: Roles of variations in meteorological parameters and anthropogenic emissions, Atmospheric Environment, 122, 839-851, 10.1016/j.atmosenv.2015.08.081, 2015.

Lu, X., Zhang, L., Chen, Y., Zhou, M., Zheng, B., Li, K., Liu, Y., Lin, J., Fu, T.-M., and Zhang, Q.: Exploring 2016-2017 surface ozone pollution over China: source contributions and meteorological influences, Atmospheric Chemistry and Physics, 19, 8339-8361, 10.5194/acp-19-8339-2019, 2019.

Ni, R., Lin, J., Yan, Y., and Lin, W.: Foreign and domestic contributions to springtime ozone over China, Atmospheric Chemistry and Physics, 18, 11447-11469, 10.5194/acp-18-11447-2018, 2018.

Pu, X., Wang, T. J., Huang, X., Melas, D., Zanis, P., Papanastasiou, D. K., and Poupkou, A.: Enhanced surface ozone during the heat wave of 2013 in Yangtze River Delta region, China, Sci Total Environ, 603-604, 807-816, 10.1016/j.scitotenv.2017.03.056, 2017.

Shu, L., Xie, M., Wang, T., Gao, D., Chen, P., Han, Y., Li, S., Zhuang, B., and Li, M.: Integrated studies of a regional ozone pollution synthetically affected by subtropical high and typhoon system in the Yangtze River Delta region, China, Atmospheric Chemistry and Physics, 16, 15801-15819, 10.5194/acp-16-15801-2016, 2016.

Su, T., Xue, F., and Zhang, H.: Simulating the intraseasonal variation of the East Asian summer monsoon by IAP AGCM4.0, Advances in Atmospheric Sciences, 31, 570-580, 10.1007/s00376-013-3029-8, 2014.

Sun, L., Xue, L., Wang, Y., Li, L., Lin, J., Ni, R., Yan, Y., Chen, L., Li, J., Zhang, Q., and Wang, W.: Impacts of meteorology and emissions on summertime surface ozone increases over central eastern China between 2003 and 2015, Atmospheric Chemistry and Physics, 19, 1455-1469, 10.5194/acp-19-1455-2019, 2019.

Tang, G., Zhu, X., Xin, J., Hu, B., Song, T., Sun, Y., Zhang, J., Wang, L., Cheng, M., Chao, N., Kong, L., Li, X., and Wang, Y.: Modelling study of boundary-layer ozone over northern China - Part I: Ozone budget in summer, Atmospheric Research, 187, 128-137, 10.1016/j.atmosres.2016.10.017, 2017.

Tie, X., Geng, F., Peng, L., Gao, W., and Zhao, C.: Measurement and modeling of O-3 variability in Shanghai, China: Application of the WRF-Chem model, Atmospheric Environment, 43, 4289-4302, 10.1016/j.atmosenv.2009.06.008, 2009.

Wang, Y., Zhang, Y., Hao, J., and Luo, M.: Seasonal and spatial variability of surface ozone over China: contributions from background and domestic pollution, Atmospheric Chemistry and Physics, 11, 351 1-3525, 10.5194/acp-11-3511-2011, 2011.

Wang, Z., Li, J., Wang, X., Pochanart, P., and Akimoto, H.: Modeling of regional high ozone episode observed at two mountain sites (Mt. Tai and Huang) in East China, Journal of Atmospheric Chemistry, 55, 253-272, 10.1007/s10874-006-9038-6, 2006.

Yang, Y., Liao, H., and Li, J.: Impacts of the East Asian summer monsoon on interannual variations of

summertime surface-layer ozone concentrations over China, Atmospheric Chemistry and Physics, 14, 6867-6879, 10.5194/acp-14-6867-2014, 2014.

Zhang, H., Wang, Y., Park, T.-W., and Deng, Y.: Quantifying the relationship between extreme air pollution events and extreme weather events, Atmospheric Research, 188, 64-79, 10.1016/j.atmosres.2016.11.010, 2017.

Zhang, Y., and Wang, Y.: Climate-driven ground-level ozone extreme in the fall over the Southeast United States, Proc Natl Acad Sci U S A, 113, 10025-10030, 10.1073/pnas.1602563113, 2016.